HIGH-FREQUENCY, HIGH-POLE COUNT DESIGN FOR IMPROVING SPECIFIC POWER DENSITY OF ELECTRIC MACHINES

BY

ANDY K. YOON

THESIS

Submitted in partial fulfillment of the requirements
for the degree of Master of Science in Electrical and Computer Engineering
in the Graduate College of the
University of Illinois at Urbana-Champaign, 2016

Urbana, Illinois

Adviser:

Associate Professor Kiruba Sivasubramaniam Haran

ABSTRACT

This thesis introduces the high frequency, high pole count (HFHP) design for improving specific power density of electric machines for weight and/or volume sensitive applications. Although electric machine designs have reached a limit in terms of efficiency, reliability, and cost, newer applications such as in aviation or the oil and gas industry are demanding next-generation motors to be lighter and more compact. The benefit of HFHP design is shown analytically by observing the effect of frequency and pole count on air-gap flux density and torque, while its adverse effects on magnetizing reactance, leakage reactance, and iron/copper losses are realized.

The concept is applied to two of the most ubiquitous electric machines today: induction machines and permanent magnet machines. Electrical equivalent circuits are utilized to analytically hypothesize the effect of HFHP designs, then finite element models (FEM) are built to verify the effects. For induction machines, significant reduction in magnetizing reactance is shown to result in growth in line current and low torque. For permanent magnet machines, however, reduction in magnetizing reactance is shown to not directly affect torque of the machine, thus increase in specific power density is shown.

The design of a 1 MW, 13 kW/kg motor is described, based on the shown benefit of HFHP design in permanent magnet machines. The motor proves that adverse effects of high frequency and high pole count are manageable by employing air-gap windings, halbach arrays, and outer rotor topology.

To my parents, my brother, and my friends,
for their love and support.

ACKNOWLEDGMENTS

This research was supported by the Grainger Center for Electric Machinery and Electromechanics (CEME) at the University of Illinois at Urbana-Champaign (UIUC), and the National Aeronautics and Space Administration (NASA). I would like to thank Professor Kiruba Haran for advising this research, and to thank my colleagues in the Power and Energy research group at UIUC for their support.

TABLE OF CONTENTS

CHAPTER 1

INTRODUCTION

Electric machines have truly become an indispensable technology, since the first patent on electric motor was obtained in 1837 [1]. From small home applications to large industrial applications, electric machines have permeated into everyday lives. Due to this fact, many types of motors have been standardized by the National Electrical Manufacturers Association (NEMA), and are left with little room for innovation. Thus, development of electric machines have unfortunately been incremental, rather than revolutionary.

However, applications for electric machines have been recently proliferating, with emergence in popularity of all-electric transportation systems, off-shore wind turbines, and harsh environment operation. While electric machines are now reaching the threshold of performance, reliability, and cost improvements, such applications necessitate further development. More specifically, improvement in specific power density of electric machines are being highlighted, as many industries are engaging in applications where minimizing volume and weight of electric motors are essential.

This thesis will first discuss reasons for shift on the focus of electric machines from conventional machines to high specific power density machines. Then, survey of current state-of-the-art power dense electric machines is presented. Then, the effectiveness of high frequency, high pole design for improving specific power density is verified. The concept is developed and challenges are realized, and the design is tested with numerical models using electrical equivalent circuit models and validated using finite element models (FEM). Two main types of electric machines are studied, which are induction machines and permanenet magnet machines.

CHAPTER 2

NEED FOR HIGH POWER DENSITY

To move toward more-electric aircrafts, development of high power dense electric motors are much demanded by the aviation industry [2], [3]. According to the Vision 2050 report by the International Transportation Association (IATA), roughly 2.4 billion passengers and 40 million tons of goods were transported in 2010. By 2050, IATA estimates a fourfold increase in number of passengers and a tenfold increase in number of amount of goods [4]. Consequently, the European Commission has estimated a 70% increase by 2020 in global aviation emissions, and 700% increase by 2050, compared to the 2005 emissions data [5]. With the price of jet fuel increasing every year, environmental and financial concerns from increasing jet fuel consumption are spurring rise in demands for expedited development in all-electric technologies in the aviation industry. While equivalent concerns have caused much progress to be made for all-electric ground transportation industry, with the state-of-the-art technology enabling up to about 270 miles of travel between charges [6], the aviation industry is still at an experimental stage with all-electric commercial airplane, with at most an hour of endurance per charge. Therefore, the aviation industry is turning toward turbo-electric propulsion technology, which utilizes energy dense fossil fuel as a source of power for electric generators while replacing jet engines with electric motors for propulsion, as shown in Figure 2.1. The cause for such an approach can

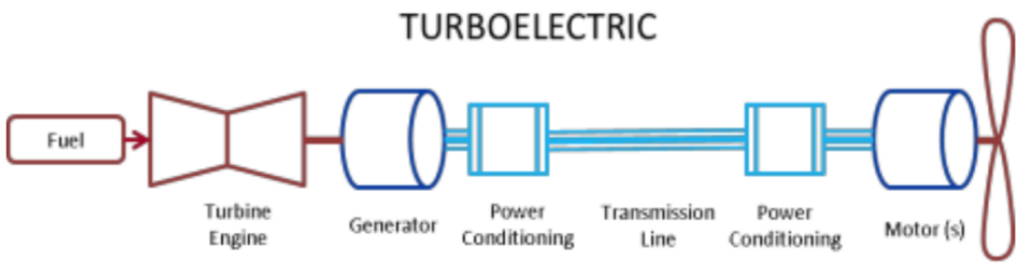

Figure 2.1: Turbo-Electric System [7]

be mainly attributed to relatively low energy density of batteries to jet fuels, and air vehicles' sensitivity to weight. Thus, development in high power dense electric machines can aid in successful implementation of such technology. In addition to high fuel efficiency, multiple advantages of turbo-electric propulsion technology are identified in [8].

Development of high power density electric machines can also prove useful in harsh environments, such as extreme temperatures or space-constrained applications. For example, electrical submersible pump (ESP) systems are used in harvesting crude oil from deep-sea environments. As of 2004, more than 100,000 ESPs are utilized worldwide, where the majority are installed across the United States, Europe, and Asia [9]. While ESPs are the second most widely used technique among three types of artificial lift system, the power consumption is known to be the highest [10]. As demand for oil continues to rise and easily-accessible oil reserves are beginning to deplete, the need for more compact motors that can provide much power is rising. Thus, improved power density for electric machines can not only lower the cost of operation for such applications, but also allow more locations to be accessible for harvesting energy.

CHAPTER 3

SURVEY ON SPECIFIC POWER DENSITY

To improve power density of electric machines, many methods are used to increase rated power of a machine or reduce the weight of the motor. Figure 3.1 shows the survey of the specific power density of electric machines of various types, through academic papers, patents, and industry websites. The surveyed types of machines are axial flux permanent magnet machines (RFPM), axial flux permanent magnet machines (AFPM), induction machines (IM), switched reluctance machines (SRM), wound-field synchronous machines (WFSM), and super conducting machines (SCM).

According to Figure 3.1, specific power densities of electric machines tend to be higher for low power machines. Also, permanent magnet machines (RFPM and AFPM) are generally observed to have higher specific power density compared to those of other machines. This is possible due to adoption of rare-earth permanent magnets as field excitation. While super conducting machines are observed to exhibit high specific power density than those of other types, note that super conducting machines are not yet a mature technology and are at a lower technology readiness level (TRL). Furthermore, induction machines can generally be observed to have low specific power densities. While its rugged structure allowes for robust and reliable operation, its relatively lower power factor and poor efficiency makes it difficult for induction machines to be designed with higher specific power density relative to other types of machines.

Note that some of the sources for the survey does not specify whether the given power is peak power or rated power, or whether the given weight is active weight or total weight. Generally, when machines have aggressive cooling techniques that involve water or oil, the auxillary weight of the cooling methods add a significant amount of weight to the overall machine. Thus, focusing on high fidelity data among the surveyed machines, it can be found that state-of-the-art, non-cryogenic electric machine in terms of

specific power density is found to be around 4 kW/kg.

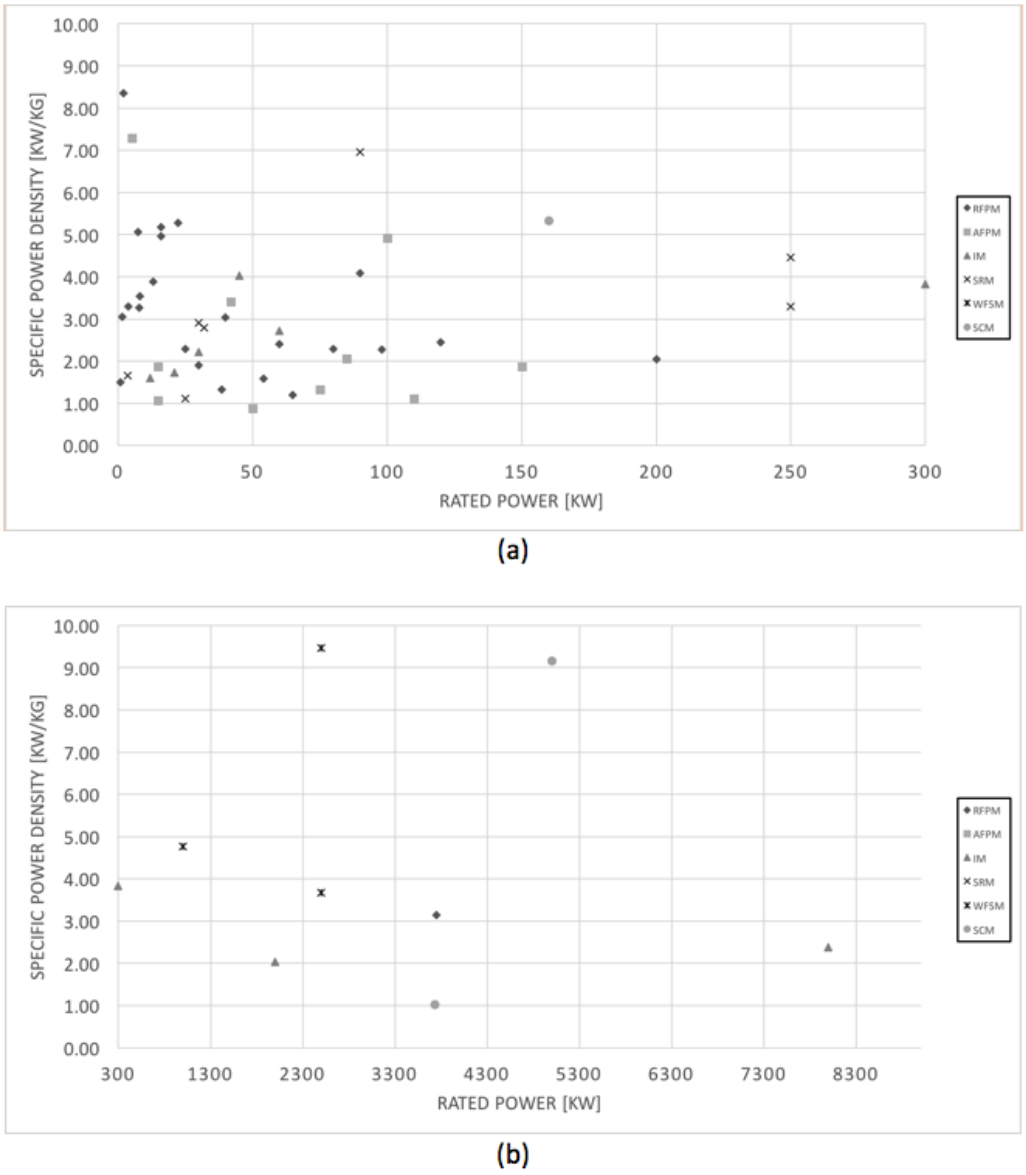

Figure 3.1: Specific Power Density for Various Electric Machines, (a) kW Rating Range and (b) MW Rating Range

CHAPTER 4

ON INCREASING SPECIFIC POWER DENSITY

Specific power density of electric machines refers to the *amount of power per unit weight*. Thus, to increase the specific power density, methods of increasing rated power or decreasing motor weight must be explored.

To increase power rating of an electric machine, high-torque or high-speed design can be considered, as mechacnical power of an electric machine is given as

$$P_{mech} = T\omega_m \tag{4.1}$$

where T and ω_m refer to mechanical torque in Nm and mechanical speed in rad/s, respectively. To identify the factors that determine torque, Lorentz force equation can be examined. The classic equation describes that the force experienced by a particle of charge, q, moving at a velocity, $\vec{v}$, across an electric field, $\vec{E}$, and a magnetic field, $\vec{B}$, is given as

$$\vec{F} = q[\vec{E} + (\vec{v} \times \vec{B})] \tag{4.2}$$

Because majority of electric machines are based on the principles of magnetic force, the magnetic term in the Lorentz force can be highlighted as

$$\vec{F_m} = \int_v (\vec{J} \times \vec{B}) dV \tag{4.3}$$

where $\vec{J}$ refers to the current density. Applying the concept of Lorentz force to electric machines, torque of an electric machine is often expressed as

$$T = 2ABV_r \tag{4.4}$$

where A, B, and V_r refer to linear current density around the airgap circumference, average flux density over the rotor surface, and rotor volume, respectively [11]. Generally, A is referred to as electric loading, and B as

magnetic loading. Thus, it is apparent that improving electrical loading, magnetic loading, or increasing the size of the machine can increase torque of a machine. However, increasing volume results in increased weight. Even if torque can be improved with larger diameter, the concurrent growth in weight will not positively affect the specific power density. Also, improvements in A and B are constrained by underlying physical factors. For example, electric loading is limited by joules losses and cooling capability. Theoretically, electric loading can be increased by pushing slot current density for a given motor further, but this presents implications as insulation failure may arise. Magnetic loading is limited mostly by material properties, such as energy density of permanent magnets and saturation flux density of steel material used for rotor and stator back yoke. Thus, significant increase in specific power density can be obtained by: (1) increasing the speed of the machine to increase power, or (2) decrease weight of the motor.

CHAPTER 5

DESIGN CONCEPT

The proposed concept aims to highly reduce the weight of the motor by moving away from the traditionally iron-intense motor topology, while leaving power of the machine unchanged. The benefit of adopting high pole design, along with the need for high frequency is discussed in this chapter.

5.1 High Pole, High Frequency

High pole count in an electric machine allows both a thinner stator and rotor yoke due to less flux per pole, which is given by

$$\phi_p = \frac{2}{P} L_{stack} D B_{peak,ag} \tag{5.1}$$

where P, L_{stack}, D, and $B_{peak,ag}$ are number of poles, stack length, air-gap diameter, and peak flux density in the air-gap. The opportunity to decrease the motor weight is clear, as doubling the pole count in a machine can reduce the yoke thicknesses by half. Furthermore, the power level can be maintained with reducing the weight if the speed is kept constant (ratio of frequency to pole count maintained) with the pole count, as rated power of a three-phase ac machine is given as

$$P_{rated} = 3 E_{rms} I_{q,rms} \tag{5.2}$$

where E_{rms} and $I_{q,rms}$ refer to induced voltage and quadrature-axis component of the stator current, respectively, and induced voltage, or back-EMF, is given by

$$E_a = K_w N_{ph} \omega_e \phi_p sin(\omega_e t) \tag{5.3}$$

where K_w, N_{ph}, ω_e, and ϕ_p refer to winding factor, number of turns per phase, electrical frequency, and flux per pole, respectively. Thus, the first order effect of high frequency, high pole count (HFHP) design in improving the

specific power density of an electric machine is realized; while increasing the number of poles allow reduction in the amount of iron, increasing frequency prevents the reduction in power level. Note that if the speed is allowed to increase, the power output can be increased.

Traditionally, high pole count motors have been widely utilized for MW-scale generators, but were forced to be made very large and slow due to unavailability of high-frequency power electronic drive capabilities. Beacuse of the same reason, high-speed motors were forced to have very low number of poles, because obtaining high frequency was difficult. However, with recent developments in power electronics and its application in variable frequency drives, frequencies higher than transmission frequency (50/60 Hz) are now easily obtained. The proposed HFHP design aims to combine the benefits of high pole count with high frequency to achieve high specific power density. However, to successfully determine the feasibility of a HFHP count design, second-order effects must be examined in detail.

5.2 Second-Order Effects of a HFHP Design

5.2.1 Magnetizing Reactance

While increasing the number of poles in a design can lead to reduced rotor and stator yoke thicknesses, the resulting changes in dimensions can affect the magnetizing reactance of a machine. Magnetizing reactance of an electric machine is given by

$$X_m = k\omega_e \left(\frac{N_{ph}}{P}\right)^2 \frac{\mu_0 \pi D L_{stack}}{2L_{ag}} \tag{5.4}$$

where k, ω_e, N_{ph}, P, D, L_stack, and L_{ag} refer to winding constant, electrical frequency, number of turns per phase, number of poles, air-gap diameter, stack length, and effective air-gap length, respectively. Note that the magnetizing reactance is proportional to $\frac{\omega_e}{P^2}$. If the speed is kept contant, magnetizing reactance is inversely proportional to P.

In synchronous machines, the magnetizing reactance constitutes a large portion of the synchronous reactance. Synchronous machines (permanent-magnet or wound-field) have separate excitation for rotor and stator, and

their performance is not directly affected by the low magnetizing reactance. Having low synchronous reactance, however, is known to cause significant amount of short circuit fault currents to flow in the stator windings, but the issue can be easily mitigated by using protection systems such as overcurrent circuit-breakers.

For induction machines, however, low magnetizing reactance leads to increased magnetizing current during operation, which can significantly lower the power factor of the machine. Thus, HFHP designs may not be undesirable for induction machines or any reluctance type machines, as low power factor leads to poor efficiency.

5.2.2 Leakage Reactance

Leakage reactance quantifies the amount of flux that does not contribute to linking of the stator windings and the rotor windings. As motor dimensions change with pole count, change in leakage reactance must also be accounted for. Major source of leakage flux in an electric motor include: (1) slot leakage reactance, (2) end-winding leakage reactance, and (3) differential leakage reactance. Slot leakage reactance stems from the phenomenon where magnetic flux leaks between the teeth and through the slots. End-winding leakage reactance is due to the end-turns in the non-active portion of a machine, and differential leakage reactance represents flux trapped in the air-gap. To observe how the number of poles and frequency affect these major types of leakage reactances, each element must be studied.

Slot reactance can be expressed as

$$X_s = k_s \omega_e L_{stack} N_{ph}^2 \left[\frac{P_{s1}}{S_1} + \frac{P_{s2}}{S2} \right] \tag{5.5}$$

where k_s, P_{s1}, P_{s2}, S_1, and S_2 correspond to geometric constant, stator slot permeance, rotor slot permeance, total number of stator slots, and total number of rotor slots, respectively, where slot permeance refers to effective ratio of slot depth to slot width [12]. Note that P_{s2} and S_2 are irrelevant for permanent magnet machines. If number of slots is assumed to be proportional to number of poles, where the slot permeance is thus also proportional to number of poles, then slot leakage reactance is proportional to frequency. If the speed is kept constant, slot leakage reactance is proportional to P. How-

ever, note that this is an upper bound of proportionality between pole count and slot leakage reactance, as myriad of slot dimensions and configurations can be considered to optimize for the minimum slot leakage flux.

End winding leakage reactance is expressed as

$$X_e = k_e \frac{\omega_e N_{ph}^2 D}{P^2} \tag{5.6}$$

where k_e refers to a constant to adjust for units. Thus, the end-winding reactance can be determined to decrease as a factor of P.

Lastly, the differential leakage reactance is shown as

$$X_{diff} = \left[\frac{\pi^2 (20 S_p^2 + 36) \sin^2(\frac{\pi}{2S_p})}{486} - 1 \right] X_m \tag{5.7}$$

where S_p refers to the number of slots per pole. Thus, considering a case where S_p is constant regardless of number of poles, differential leakage reactance can be said to be proportional to magnnetizing reactance, which is inversely proportional to the number of poles.

While end-winding leakage reactance and differential leakage reactance is observed to decrease with increasing number of poles, slot leakage reactance is shown to increase with number of poles, assuming number of slots per pole is kept constant. However, the relationship between the pole count and overall leakage reactance must be fully studied as some leakage components might be more prominent than others.

5.2.3 Iron losses

Iron loss, which results from both eddy currents and magnetic hysteresis, can be characterized by

$$P_{iron} = P_{eddy} + P_{hysteresis} = \beta f^2 B^2 + \alpha f B^\gamma \tag{5.8}$$

where P_{iron}, B and f refer to iron loss density, flux density and frequency, respectively. α, β, γ refer to empirical coefficients which can vary with materials used and various design configurations [13]. The equation clearly shows that the iron loss density grows significantly with frequency, but the effect may possibly be alleviated by thickness reduction in both stator and rotor

iron with the adoption of a HFHP design.

In addition to conventional ways of reducing iron losses, such as the use of laminated or thin-filmed soft magnetic materials, stator teeth can be eliminated and air-gap winding configuration can be adopted. Traditionally, the winding is fit inside a slot formed by the stator back yoke and the stator teeth. As teeth is usually one of the regions in a machine with highest flux density, elimination of teeth would not only further decrease the weight of the motor, but also eliminate associated iron losses. Thus, air-gap winding topology can significantly lower the risk of high iron losses due to high frequency, and reduce weight, as shown in Figure 5.1.

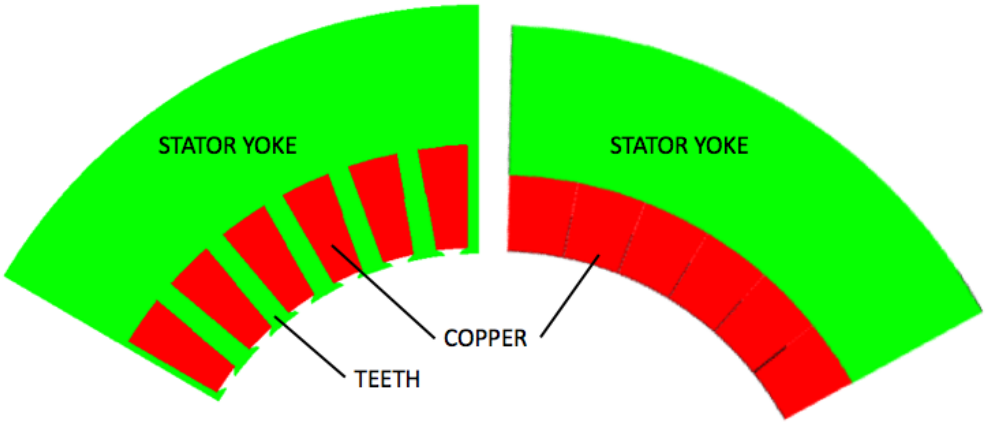

Figure 5.1: Demonstration of Air-Gap Winding

By adopting air-gap winding configuration, the volume once occupied by iron teeth can be utilized to make the winding area wider, and radial depth shorter as shown in Figure 5.1. Along with reduced iron yoke thickness for high-pole designs, this presents an opportunity for increased electrical loading due to thermal benefits. However, note that detailed studies for its effect in magnetizing reactance and leakage inductance must be performed, as conventional relationships described in Equations 5.3 - 5.7 are inapplicable.

Furthermore, in case of PMSM, Halbach arrays can be adopted to completely eliminate the rotor back yoke. Typically, magnets in a surface permanent magnet machines are oriented radially inward or outward to establish flux density in the air-gap. This requires a sufficient amount of iron to retain flux in the rotor back yoke. If the magnets are arranged in a Halbach array, the flux can be canceled on one side, thereby eliminating the heavy iron yoke

[14]. In Figure 5.2, an example of Halbach array arrangement demonstrates the flux cancellation.

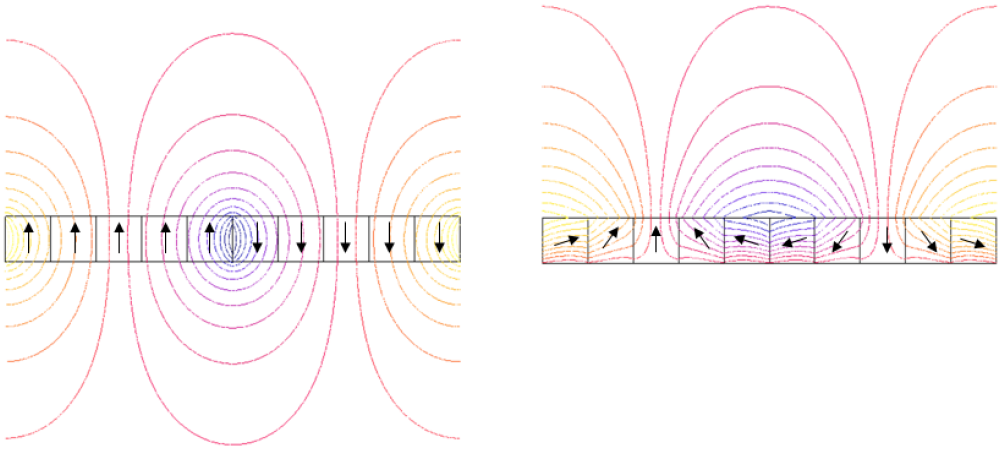

Figure 5.2: Conventional Magnet Arrangement Flux Lines (left) and Halbach Array Arrangement Flux Lines (right)

5.2.4 Copper Losses

When alternating current is carried by a conductor, current density tends to be higher closer to the surface of the conductor. Consequently, the effective resistance grows, and the corresponding losses can be roughly calculated as

$$P_{ac} = \frac{B_p^2 \omega_e^2 d^2}{32\rho} \tag{5.9}$$

where B_p, d, and ρ refer to peak flux density, copper diameter, and copper resistivity, respectively [15]. While P_{ac} can be observed to grow significantly with frequency, reducing the diameter of the conductor can negate the effect. Thus, the problem can be addressed by employing Litz-wire, which divides each phase winding into high number of smaller-diameter conductors in parallel.

CHAPTER 6

HFHP INDUCTION MACHINE

Standard induction machines have been utilized for over 100 years due to simplicity in manufacturability, robustness in performance, and reliability. Control of induction motors also add to its many benefits, as induction machines are able to naturally adapt to the changing load. Thus, improvements in power density of induction machines can be much beneficial to many industrial applications. This chapter aims to examine the feasibility of HFHP IM through the use of analytical method and finite element analysis. A 5 horsepower induction machine from WEG Industries is chosen as a baseline for the study, and is shown in Figure 6.1. The nameplate of the motor is shown in Figure 6.2.

Figure 6.1: A 5 HP Induction Machine Used for the Study

6.1 Induction Machine Equivalent Circuit Formulation

The per-phase electric equivalent circuit for induction machines are generally depicted as shown in Figure 6.3, where R_s, X_{ls}, X_m, R_c, X'_{lr}, R'_r, and s rep-

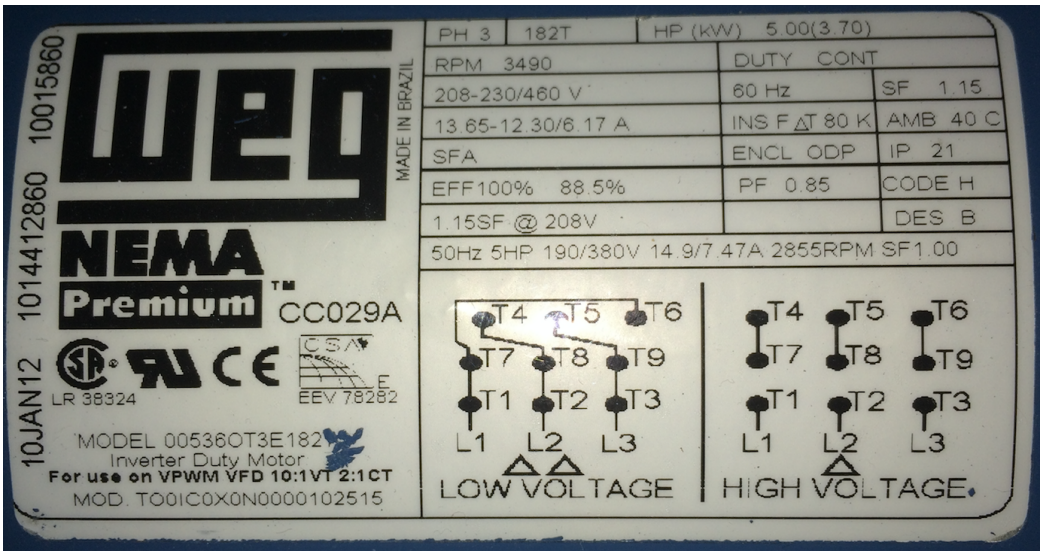

Figure 6.2: Nameplate of the 5 HP Motor

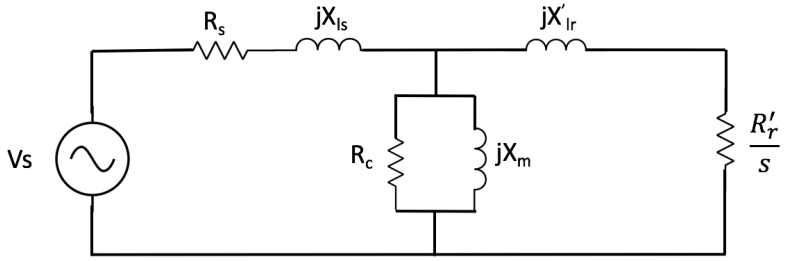

Figure 6.3: Induction Machine Equivalent Circuit

resent stator winding resistance, stator leakage reactance, magnetizing reactance, core loss resistance, rotor leakage reactance, rotor winding resistance, and slip, respectively. To find the resulting torque with changing equivalent circuit parameters (with pole count), the Thevenin equivalent circuit can be derived as shown in Figure 6.4. The expressions for the Thevenin equivalent voltage and impedance are shown in Equations 6.1 and 6.2, respectively.

$$V_{th} = V_s \frac{\frac{jX_m R_c}{R_c + jX_m}}{\frac{jX_m R_c}{R_c + jX_m} + R_s + jX_{ls}} \tag{6.1}$$

$$Z_{th} = \frac{jX_m R_c (R_s + jX_s)}{R_s + R_c + j(X_s + X_m)} \tag{6.2}$$

Mechanical torque can thus be found by dividing mechanical power in the rotor resistance element with mechanical speed. Mechanical torque is given

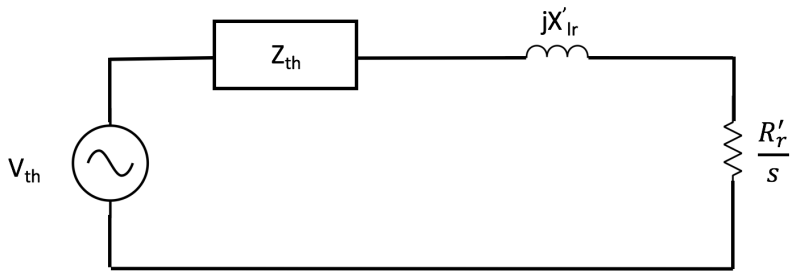

Figure 6.4: Induction Machine Thevenin Equivalent Circuit

in Equation 6.3.

$$T_{mech} = (\frac{P}{2\omega_e}) \left[\frac{3V_{th}^2}{(R_{th} + R_r'/s)^2 + (X_{th} + X_{lr}')^2} \right] \frac{R_r'}{s} \tag{6.3}$$

Because the rating of the machine is dependent on its thermal properties, line current must be examined for each design to determine the rated slip. Line current can be simply be found by deriving the input impedance of the machine, and dividing the quantity by input voltage. Equation 6.4 shows how the input impedance can be calculated.

$$Z_{in} = R_s + jX_l s + \frac{(R_r'/s + jX_{lr}') \frac{jX_m R_c}{R_c + jX_m}}{R_r'/s + jX_{lr}' + \frac{jX_m R_c}{R_c + jX_m}} \tag{6.4}$$

To determine the equivalent circuit parameters for the baseline 5 HP motor, bench tests were performed as described in the IEEE standard procedure for polyphase induction motors and generators [16]. The results are shown in Table 6.1. Note that the ratio of stator leakage reactance and rotor leakage reactance is chosen as 0.67 because the nameplate of the baseline motor specified that the motor belonged in class B.

From the obtained parameters, along with Equations 6.3 and 6.4, the rated mechanical torque and the rated line current can be calculated as 10.79 Nm and 12.68 A, respectively. With 6% and 3% error for mechanical torque and line current, respectively, the equivalent circuit analysis is in congruence with the nameplate data shown in Figure 6.2. The possible source of error may be from the blocked-rotor and no-load test, where approximations were made for calculating the parameters. For example, stator conduction losses and leakage were omitted when calculating the shunt elements for the no-

Table 6.1: Equivalent Circuit Parameters for the Baseline Induction Machine

Parameter	Value	Units
R_s	0.395	Ω
R'_r	0.35	Ω
X_{ls}	0.66	Ω
X'_{lr}	0.98	Ω
X_m	28.41	Ω
R_c	175.5	Ω

load test, and the shunt elements were ignored when calculating the series elements from the blocked-rotor test. Note that for more accurate calculation of parameters, an iterative method should be adopted, as specified in the IEEE standard procedure for polyphase induction motors and generators. As this study focuses on changes between designs, the parameters obtained is determined to be sufficient.

6.2 Analytical Method

To determine the effect of high frequency and pole count on induction machine torque, each parameter must be examined closely. In section 5.2, it was discussed that magnetizing reactance, X_m is inversely proportional to the number of poles. Also, it was discussed that some leakage reactance elements are proportional to number of poles, while some are inversely proportional to number of poles. Stator and rotor winding resistances are expected to be unchanged. Note that core loss resistance is neglected in this study for an easier comparison of design between the designs.

To determine the ratio of various leakage reactance terms that make up the total leakage reactance, Equations 5.5 - 5.7 are examined. With the geometric measurements, the ratio of slot leakage reactance, end leakage reactance, and differential leakage reactance are determined as 0.5, 0.3, and 0.2, respectively. The parameters shown in Table 6.1 are used, along with Equation 6.3, to predict the effect of high frequency and high pole count design on induction machines. Values of stator and rotor equivalent resistance was not changed, whereas magnetizing reactance and end leakage reactance

was allowed to change inversely proportional to number of poles. Slot leakage reactance and differential leakage reactance was allowed to increase proportionally with number of poles. The ratio of stator leakage reactance and rotor leakage reactance is assumed to be propated through HFHP designs. Figure 6.5 shows the change in reactances with increasing number of poles. Figure 6.6 includes line current and mechanical torque for various designs with respect to slip. In Figure 6.6a, it is obvious that the magnitude of current increases as the pole count and frequency is increased around zero slip, due to low magnetizing reactance compared to leakage reactance. Figure 6.6b shows that the breakdown torque decreases with increasing number of poles and frequency. To determine the rated torque for various designs, the slip at which rated current is observed is found, assuming that slot current density has to be maintained for thermal limits. Note that this assumption disregards the reduction in thickness of the stator yoke due to increased pole count. Because of the thinner stator yoke and thus reduced thermal resistance, slightly higher current density is expected to be allowed. The results for rated torque and slip are shown in Table 6.2, along with the ratio of stator leakage reactance and magnetizing reactance.

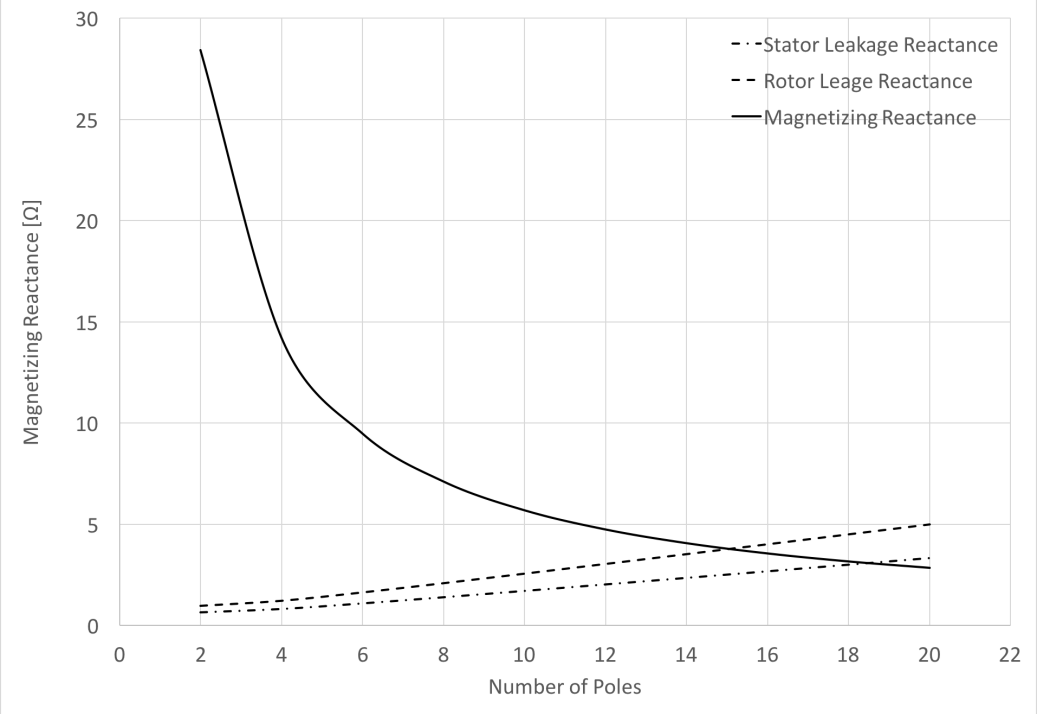

Figure 6.5: Change in Motor Equivalent Reactances with Pole Count

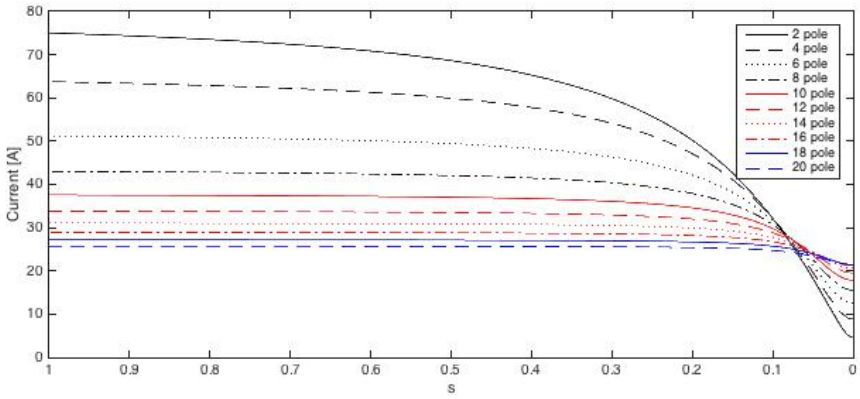

(a) Line Current

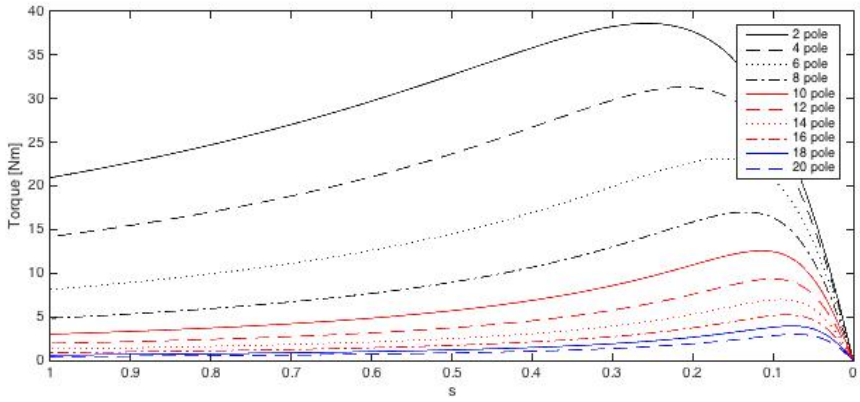

(b) Mechanical Torque

Figure 6.6: Line Current and Mechanical Torque for Various Pole Count (Analytical Results)

The results in Table 6.2 show that rated torque rapidly decreases after pole count exceeds four for the particular induction machine. The reason is attributed to the growing ratio between stator leakage reactance and magnetizing reactance. For designs with pole count higher than four, the ratio exceeds 0.1. This growth of ratio and concurrent reduction of magnetizing reactance results in greater magnetizing current needed for the same amount of torque.

6.3 Finite Element Model Analysis

The designs that were explored analytically in section 6.2 are built using a finite element modeling tool, Flux2D, and are analyzed using finite element

Table 6.2: Rated Slip and Rated Torque for Various Pole Count Choices

Pole Count	Frequency[Hz]	Rated Slip	Rated Torque[Nm]	X_{ls}/X_m
2	60	0.0306	10.84	0.0232
4	120	0.0225	7.62	0.0581
6	180	$< 10^{-5}$	0.0032	0.1162
8	240	$< 10^{-5}$	0.0028	0.1975
10	300	$< 10^{-5}$	0.0024	0.3020
12	360	$< 10^{-5}$	0.002	0.4298
14	420	$< 10^{-5}$	0.0016	0.5808
16	480	$< 10^{-5}$	0.0013	0.7550
18	540	$< 10^{-5}$	0.001	0.9525
20	600	$< 10^{-5}$	0.0008	1.1732

analysis. While the electric equivalent circuit is sufficient for most analysis, finite element analysis (FEA) can more accurately capture the magnetic changes that occur due to increase in frequency and pole count.

To build a 2D finite element model (FEM) that accurately represents the baseline machine, the machine was cut so that the motor's cross section can be examined and exact dimensions measured. Figure 6.7 shows the cut pieces of the motor used for measurements. Key dimensions are tabulated in Table 6.3.

Table 6.3: Key Dimensions of the Baseline IM

Parameter	Value	Units
Stator Outer Radius	91.3972	mm
Air Gap Length	0.7	mm
Air Gap Radius	49.4972	mm
Stator Yoke Thickness	23.2	mm
Teeth Radial Depth	18	mm
Teeth Thickness	3.65	mm
Shaft Radius	15	mm
Active Length	70.21	mm
Number of Poles	2	-
Number of Turns per Slot	58	turns

Based on the key dimensions, geometrically accurate FEM is built, as shown in Figure 6.8. Equivalent circuit parameters for the FEM is extracted

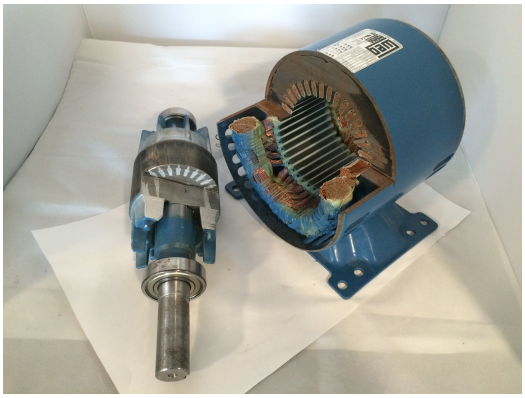

(a) Motor, Disassembled and Cut

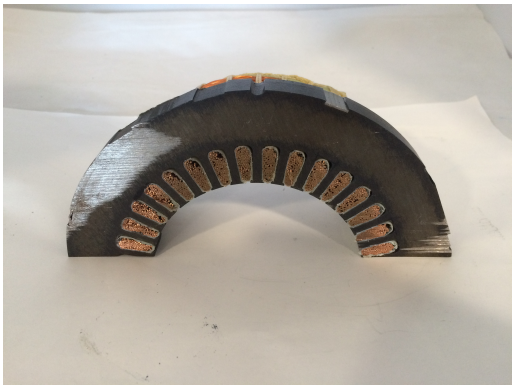

(b) Stator Cross Section Area

(c) Rotor Cross Section Area

Figure 6.7: Baseline Motor Cut Pieces for Finite Element Model Formulation

using no-load and blocked-rotor equivalent test scenarios and the results are shown in Table 6.4. The resulting rated torque and rated current are 10.17 Nm and 11.6 A, respectively. Note that the torque and current values are 0.5% higher and 5% lower, respectively. The slight error in current is expected, as core loss term is neglected in the FEM. Furthermore, some dimensions, specifically air-gap length, may not be accurate due to the small value and the resulting high possibility of measurement error.

Figure 6.9 shows the modified models for higher frequency and higher pole count designs. Note that stator and rotor iron yoke thicknesses are reduced as higher number of poles are adopted. Furthermore, the number of turns per slot are scaled inversely with pole count to address geometric constraints (reduced slot dimensions) and thermal constraints. As observed in Figure 6.9, peripheral dimensions are also scaled inversely with pole count to maintain number of rotor bars and stator slots per pole, to ensure that equivalent

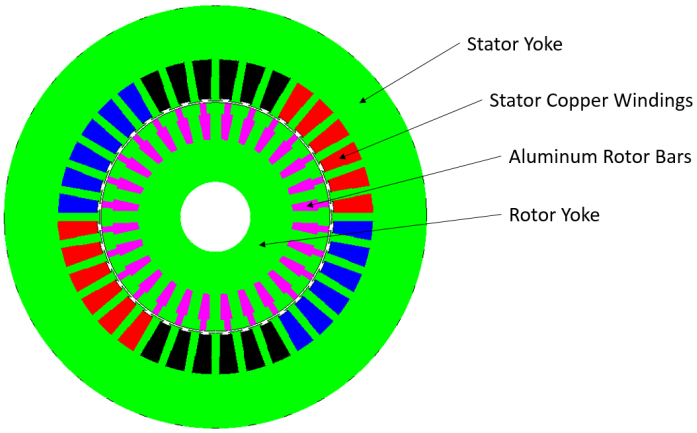

Figure 6.8: Baseline Induction Machine Finite Element Model

circuit parameters are only dependent on the pole count.

Table 6.4: Equivalent Circuit Parameters for the Baseline FEM

Parameter	Value	Units
R_s	0.394	Ω
R'_r	0.37	Ω
X_{ls}	0.69	Ω
X'_{lr}	1.04	Ω
X_m	27.1	Ω
R_c	-	Ω

The results of FEA are shown in Figure 6.10. While the analytical results and FE results do not exactly match, the similarity in general trend is observed. With increasing pole and frequency, line current increases, while breakdown torque decreases. The inconsistency between equivalent circuit analysis and FEA can be attributed to a few reasons. First of all, Equations 5.4, 5.5, 5.6, and 5.7 may not entirely capture the physical characteristic of the flux traversing through the machine. Thus, assumptions regarding proportionality with pole count with such parameters may not be entirely accurate. Second of all, the ratio of stator leakage reactance and rotor leakage reactance that was chosen for the baseline design was assumed constant among the designs. However, observing the torque-slip curve shown in Figure 6.10b suggest that higher pole count designs show characteristics of the "C" class, where breakdown torque is medium and starting torque is com-

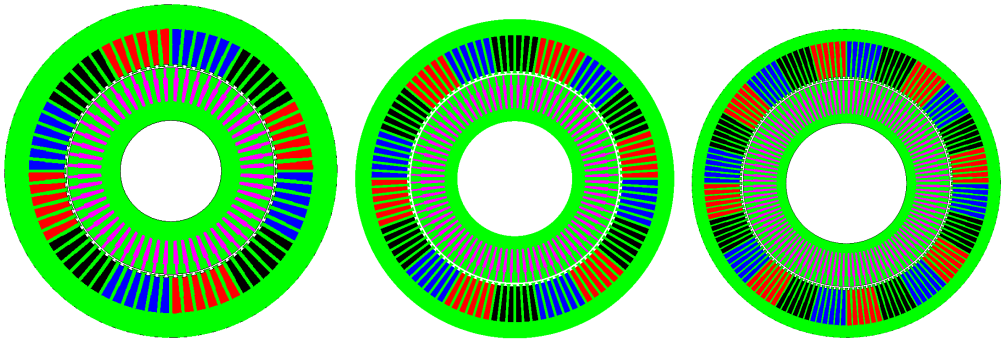

(a) 4 pole, 120 Hz (b) 6 pole, 180 Hz (c) 8 pole, 240 Hz

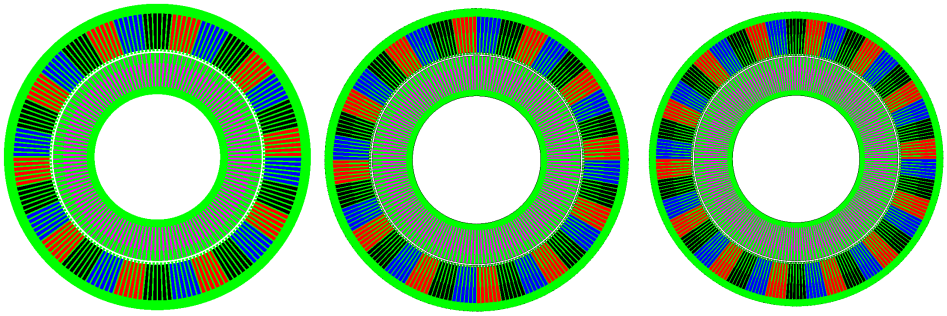

(d) 10 pole, 300 Hz (e) 12 pole, 360 Hz (f) 14 pole, 420 Hz

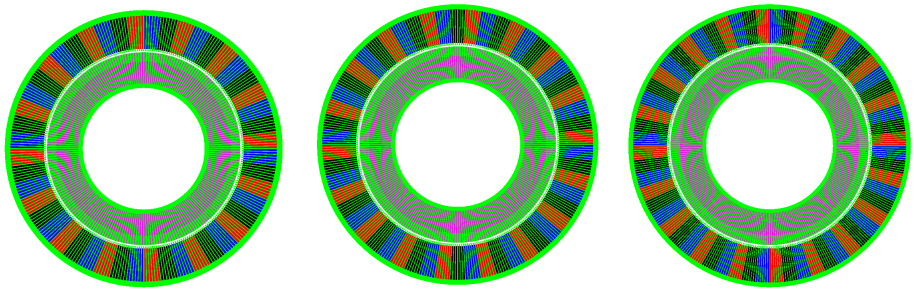

(g) 16 pole, 480 Hz (h) 18 pole, 540 Hz (i) 20 pole, 600 Hz

Figure 6.9: Finite Element Models for HFHP Induction Machine Case Study

parable to the breakdown torque. Thus, the ratio between the two leakage reactance terms may have changed across the designs. Nevertheless, the analytical method successfully predicted the behavior and performance of high pole high frequency induction machines, as evidenced by the FEA results.

The results shown in Figure 6.10 are examined to find the rated slip for each design. Then, the rated torque is extracted from the torque-slip curve. The two information are used to calculate the corresponding rated power. Then, specific power density is determined by extracting volume data from the FE models. The power density results are shown in Table 6.5. Note that typical

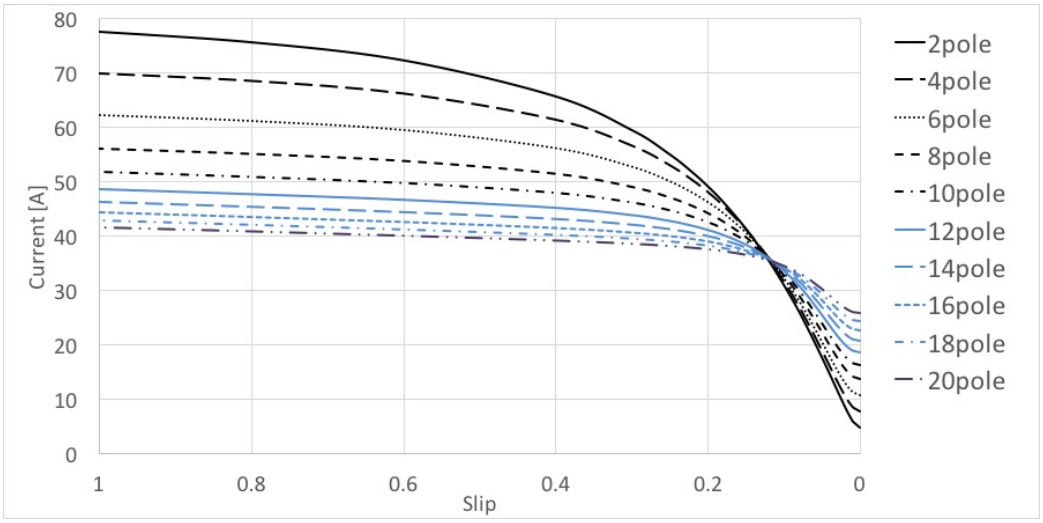

(a) Line Current

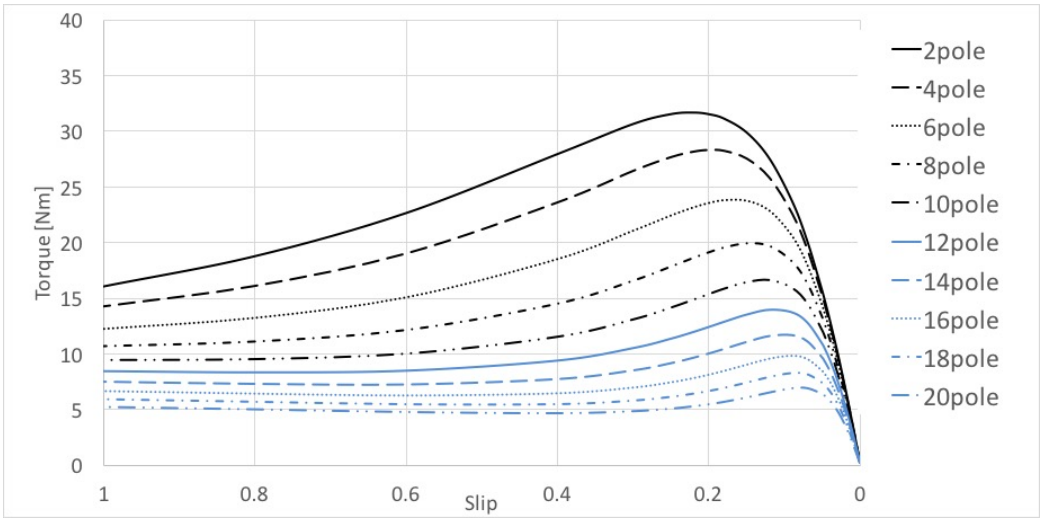

(b) Mechanical Torque

Figure 6.10: Line Current and Mechanical Torque for Various Pole Count (FEA Results)

densities of 5900 kg/m^3, 8960 kg/m^3, and 2700 kg/m^3 are chosen for iron, copper, and aluminum, respectively. While a 20% drop in rated torque from a two-pole design to a four-pole design is observed, power density is observed to increase by 10%. While this demonstrates the effectiveness of a HFHP design, induction machines' decrease in magnetizing reactance with increasing pole count proves undesirable for improving specific power density. Furthermore, starting with the eight-pole design, rated line current is observed to be unobtainable. However, growth in leakage reactance and thus growth in ratio of stator leakage reactance to magnetizing reactance can be avoided if proper

Table 6.5: Rated Slip, Rated Torque, and Specific Power Density for Various Pole Count Choices (FEA Results)

Pole Count -	Frequency [Hz]	Rated Slip -	Rated Torque [Nm]	Power Density [kW/kg]
2	60	0.0306	10.18	0.339
4	120	0.0241	7.99	0.372
6	180	0.0116	3.84	0.207

number of slots per pole is used. For example, note that the analytical and FE studies which are presented only considers a case where the peripheral dimensions of the stator and the rotor are scaled down with increasing pole count (number of stator and rotor slots per pole maintained) for ease of comparison. However, further increase in power density is expected with proper optimization of slot dimensions for various pole count-frequencies.

Table 6.6: Rated Slip, Rated Torque, and Specific Power Density for Various Pole Count Choices (FEA Results), with Motor Outer Diameter Maintained

Pole Count -	Frequency [Hz]	Rated Slip -	Rated Torque [Nm]	Power Density [kW/kg]
2	60	0.0306	10.18	0.339
4	120	0.0436	16.824	0.670
6	180	0.0380	15.173	0.635
8	240	0.0337	13.343	0.577
10	300	0.0295	11.41	0.506
12	360	0.0251	9.43	0.426
14	420	0.0201	7.34	0.337
16	480	0.0139	4.96	0.232

In addition, note that the air-gap diameter was chosen as a reference among the designs so that magnetizing reactance was only affected by pole count for fair comparison. However, if the outer diameter of the stator is to be kept as a constant, rise in magnetizing reactance and thus torque is expected due to expansion of air-gap diameter (note that Equation 5.4 shows that magnetizing reactance is inversely proportional to pole-count, but proportional to air-gap diameter). However, FE analysis is required to quantify the ef-

fectiveness of maintaining outer diameter on specific power density because the overall weight will increase as well. Table 6.6 shows the effectiveness of keeping machine's outer diameter as a reference. In such a case, the decrease in magnetizing reactance is alleviated, while torque rises. Note that compared to the case where air-gap diameter was kept as a reference, where higher-than-eight-pole-count designs were unable to meet the specified line currents, the case where keeping outer diameter as a reference is able to meet such requirements up to 16 poles. Furthermore, while the case study is performed with line current magnitude maintained, the growth in slot area is not accounted for. Theoretically, more line current is allowed with bigger slot area for constant slot current density. Thus, the rated torque values observed in Table 6.6 is expected to be at most 5% higher, based on the change in slot area.

CHAPTER 7

HFHP PERMANENT MAGNET MACHINE

Generally, permanent magnet synchronous machines (PMSM) have relatively higher specific power density compared to those of other types of machines. Thus, permanent magnets are ubiquitous in transportation systems, specifically in aerospace applications. Nevertheless, current permanent magnet machines still use conventionally low number of poles and close-to-transmission frequency. This chapter explores the feasibility of HFHP design for permanent magnet machines.

7.1 Permanent Magnet Synchronous Machine Equivalent Circuit Parameters

The electrical equivalent circuit of synchronous machine is given by Figure 7.1, where E_a, X_s, and R_a represent back-EMF, synchronous reactance, and armature resistance, respectively. The back-EMF represents the voltage induced by the field excitation flux, which is proportional to the mutual inductance between the armature and field. Synchronous reactance refers to the combination of machine self-reactance and armature leakage reactance.

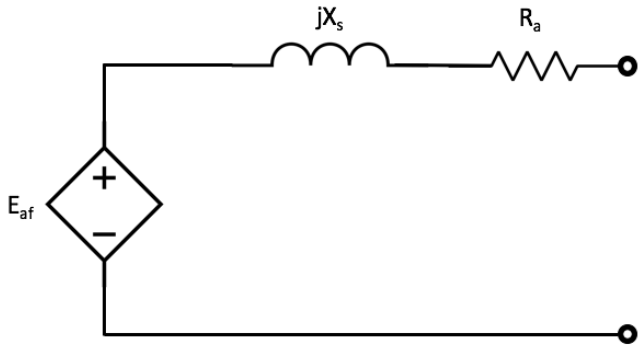

Figure 7.1: Synchronous Machine Equivalent Circuit

As discussed in Chapter 5, maintaining speed of the machine theoretically ensures that back-EMF does not drop with increasing poles, but synchronous reactance is expected to decrease with increasing pole count. With the use of permanent magnets as its field, rated power of PMSMs are expected to be unaffected by increasing number of poles as induction machines are. However, pole pitch decreases with increasing number of poles, which may increase the leakage between the magnets. Thus, the coupling between the armature and the field is expected to decrease with increasing pole count, and decrease in rated power is expected.

7.2 Finite Element Model Analysis

To quantify the feasibility of a HFHP PMSM design, a FEM is formulated using the geometry of the baseline induction machine. For a better comparison, stator of the PMSM FEM is made identical to that of the baseline IM, but the rotor is simply reconstructed with an iron yoke and permanent magnets. The baseline model for the PMSM is shown in Figure 7.2. Note that

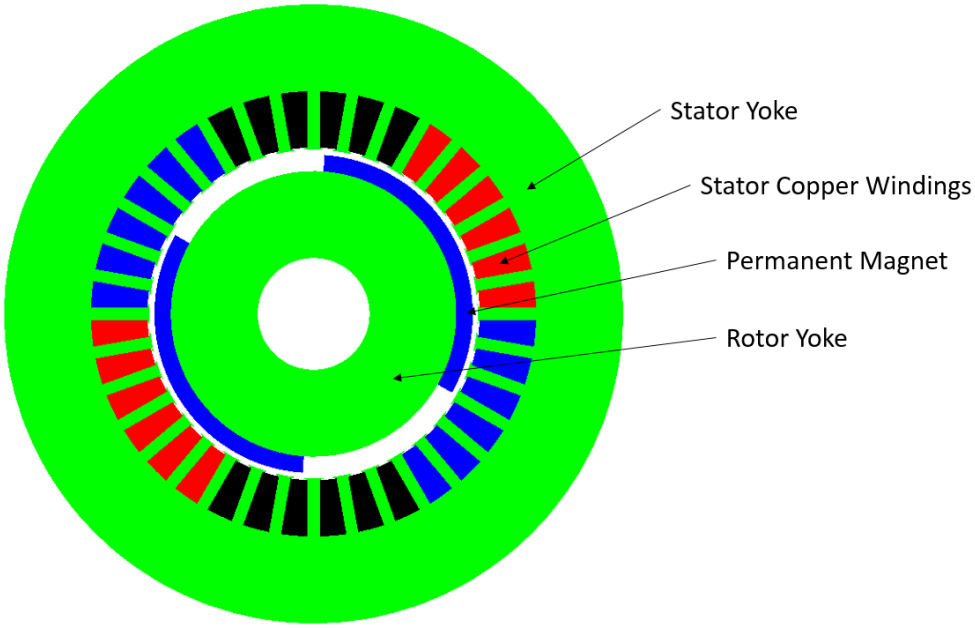

Figure 7.2: Baseline Permanent Magnet Synchronous Machine Finite Element Model

the slot current density is kept constant as the baseline induction machine

case because the thermal equivalent circuit does not change. The resulting rated torque of the baseline is found to be 12.09 Nm, which is higher than the induction machine torque due to the use of neodymium magnets, which are known for its high energy density. Figure 7.3 shows the models for higher frequency and higher pole count designs. The models were modified from the baseline PM machine by reducing the thickness of the stator yoke, rotor yoke, and the stator teeth proportionally with the number of poles. Note that the air-gap diameter was maintained across the designs.

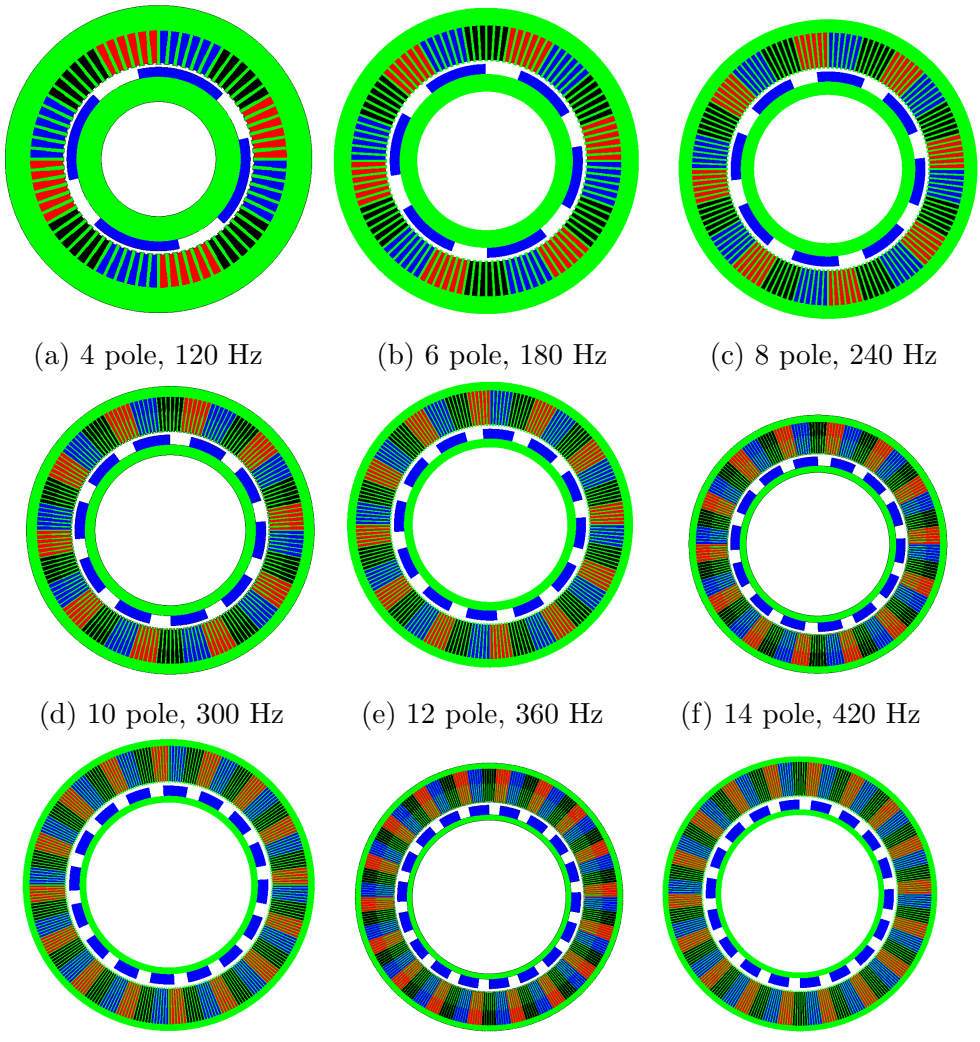

(a) 4 pole, 120 Hz (b) 6 pole, 180 Hz (c) 8 pole, 240 Hz

(d) 10 pole, 300 Hz (e) 12 pole, 360 Hz (f) 14 pole, 420 Hz

(g) 16 pole, 480 Hz (h) 18 pole, 540 Hz (i) 20 pole, 600 Hz

Figure 7.3: Finite Element Models for HFHP PMSM Case Study

Table 7.1 shows the resulting power and weight of the case study, using density values of 7300 kg/m^3, 5900 kg/m^3, and 8960 kg/m^3, for permanent

magnet, steel, and copper, respectively.

The values of power, weight, and specific power density is plotted in Figure 7.4. In Figure 7.4a, power is observed to reduce by 5% by employing 20 poles and 600 Hz fundamental frequency. This reduction can be attributed to the

Table 7.1: FEA Results for HFHP PM Machine Case Study with Air-gap Flux Density ("B"), and the Ratio of Pole Pitch to Air-gap Length ("α/g")

Pole Count -	Frequency [Hz]	Power [kW]	Weight [kg]	SPD [kW/kg]	B [T]	α/g -
2	60	4.558	11.69	0.390	0.778	101
4	120	4.757	7.871	0.604	0.779	50.7
6	180	4.772	6.599	0.723	0.777	33.8
8	240	4.747	5.963	0.796	0.772	25.3
10	300	4.702	5.581	0.843	0.766	20.3
12	360	4.644	5.326	0.872	0.757	16.9
14	420	4.576	5.145	0.889	0.748	14.5
16	480	4.499	5.008	0.898	0.736	12.7
18	540	4.416	4.902	0.901	0.724	11.3
20	600	4.326	4.817	0.898	0.711	10.1

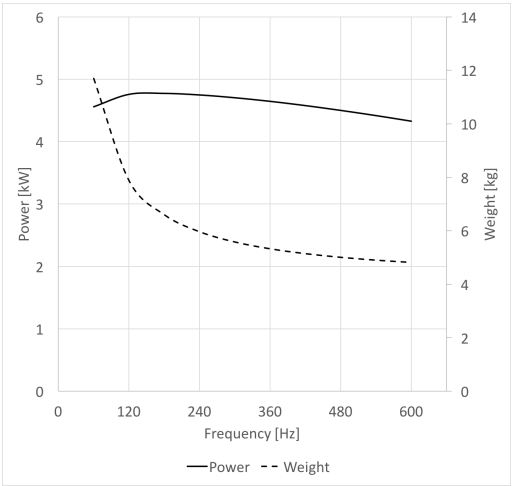

(a) Power and Weight

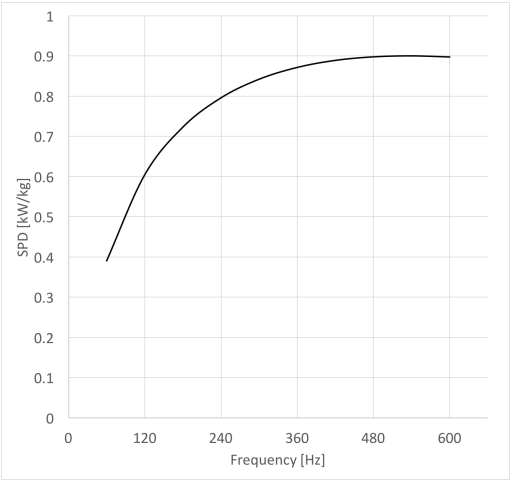

(b) Specific Power Density

Figure 7.4: HFHP PM Machine Case Study Results

increase in leakage flux between the magnets due to the decrease in ratio of pole pitch to air-gap length with pole count. In Table 7.1, normal component of the peak flux density in the air-gap is reduced by 8.6% for the 20-pole, 600

Hz design. Nevertheless, the benefit of adopting HFHP topology is clearly visible in Figure 7.4b. Specific power density of the PM motor is observed to double by increasing the pole count and frequency tenfold.

Furthermore, as keeping the outer diameter of the motor and its effectiveness in improving specific power density of induction motors was observed, the 20-pole, 600 Hz design of the PM machine is chosen to study the phenomenon. To account for the growth in air-gap diameter and thus growth in stator slot area, line current magnitude is increased by a factor of 1.6 to keep the slot current density constant. Figure 7.5 shows that while the weight of the machine increases from 4.82 kg to 7.02 kg due to the expanding diameter, the torque is observed the increase from 11.48 Nm to 24.18 Nm, thus increasing the specific power density by 44.7%.

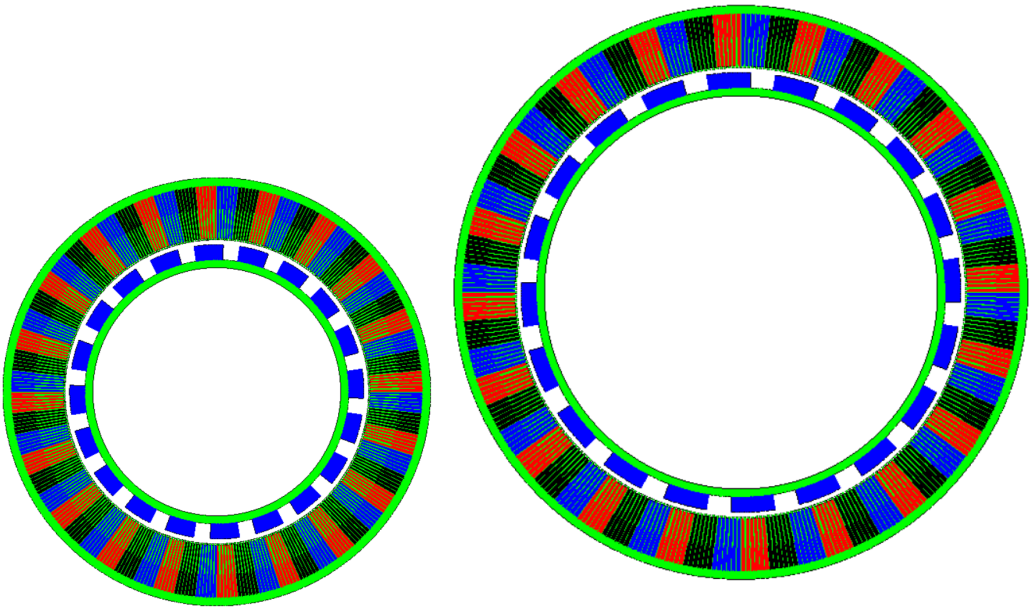

(a) Torque: 11.48 Nm
Total Weight: 4.82 kg
SPD: 0.898 kW/kg

(b) Torque: 24.18 Nm
Total Weight: 7.02 kg
SPD: 1.30 kW/kg

Figure 7.5: Power Density Difference between (a) Air-Gap Diameter Reference and (b) Outer Diameter Reference

7.3 Example of HFHP PM Machine

While the case study performed in section 7.2 considers only the first-order effects of high freqency and high pole count along with leakage reactance effects, this section presents a PM machine that is being developed as a part of a project funded by NASA. The concept of HFHP design along with methods described in Section 5.2 (Halbach arrays, air-gap winding, outer rotor topology, and Litz wire) are applied to design and test a 1 MW rated PM machine with a specific power density and efficiency goals of >13 kW/kg and > 96%, respectively. From the baseline design of 3 kHz, 10 pole-pair machine with outer diameter and active length of 12.2 inches and 15 inches, respectively, a set of optimization efforts were made to determine the appropriate copper depth, magnet and stator yoke depth, and wire gauge dimensions. Detailed methods used for the optimization can be found in [17]. Figure 7.6 shows the final design of the 1 MW motor. Note that while the effect of high frequency

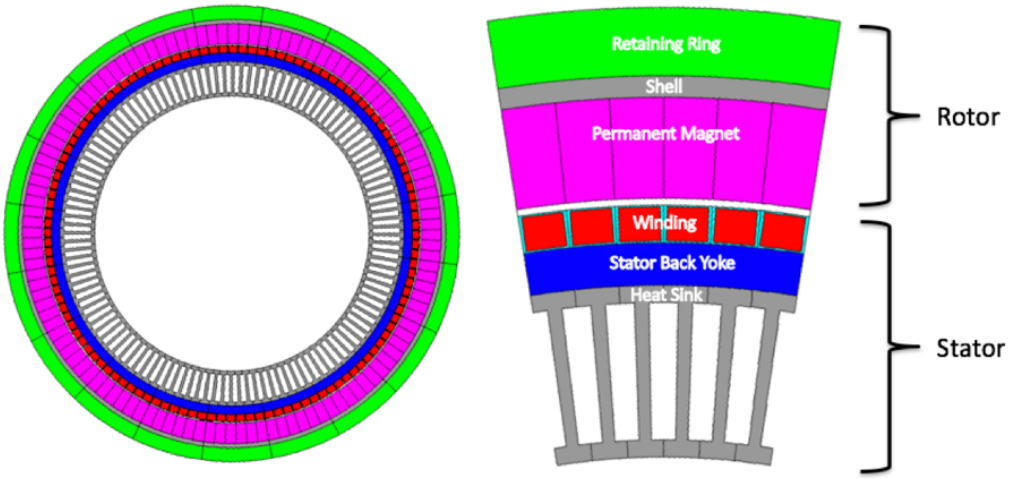

Figure 7.6: An Axial View of the HFHP Motor

on core losses are not included in the case studies, the efficiency of this motor demonstrates that the significant reduction in core material in the design aids in reduction of the overall iron losses. Tables 7.2 and 7.3 summarize loss breakdown and weight breakdown, respectively.

While core losses and copper losses were expected to be significant for high-frequency, high pole count designs, Table 7.2 suggests that careful optimization and adoption of appropriate topologies can decrease such losses significantly. Furthermore, the effectiveness of the high frequency, high pole

Table 7.2: Losses

Copper Losses	5.28	kW
Iron Losses	1.5	kW
Windage Losses	9-20	kW
Bearing Losses	1	kW
PM Losses	0.4	kW
Total Losses	17.2 - 28.2	kW
Efficiency	97.2-98.3	%

Table 7.3: Weight Breakdown

Retaining Ring	9.46	lb
Inconel Shell	35.23	lb
Permanent Magnet	48.74	lb
Copper	24.09	lb
Stator Yoke	19.51	lb
Ground Cylinder & Heat Sink	18.2	lb
Bearing retainers & rings	0.454	lb
Bearings	3.059	lb
Bolts	0.0324	lb
Total Weight	156.4	lb
Power Density	14	kw/kg

count design is demonstrated in Table 7.3, where specific power density of 14 kW/kg is shown.

CHAPTER 8

CONCLUSION

As people are becoming more environmentally aware, advancements in electric transportation and clean energy source have become increasingly important. At the base of electric transportation technology, electric machines can provide propulsion at very high efficiency. With air vehicles' apparent sensitivity to weight, improvements in specific power density of electric machines can expedite a successful implementation of electric air vehicles. Furthermore, as off-shore wind is being highlighted with great potential for much energy due to higher availability of stronger wind speeds, electric machines with improved specific power density is expected to aid in reducing the challenges and risks in off-shore wind farm constructions.

This thesis proposed high-frequency, high pole count (HFHP) topology for improving power density of induction machines and permanent magnet synchronous machines. The benefit of HFHP design is realized, as adopting high pole count presents an opportunity to significantly reduce the amount of heavy alloy needed in electric machines, if frequency is allowed to increase for constant speed. However, adverse second-order effects, such as increased iron loss density, increase in copper losses, reduced magnetizing reactance, and increase in leakage reactance, are realized.

The HFHP concept is applied to induction machines, both through electrical equivalent circuit models and finite element models, based on a baseline, off-the-shelf induction machine. The results from the electrical equivalent ciruit shows that the increase in leakge reactance, decrease in magnetizing reactance, and the resulting growth in the ratio of leakage to magnetizing reactance cause the line current to increase beyond the rated current of the baseline machine for higher pole counts and frequencies. Finite element analysis confirms the phenomenon, where the decrease in torque outweighs the benefit of reduced amount of steel. For second iteration of the case study, outer diameter is kept as a referene and air-gap diameter is allowed to in-

crease with increasing pole count and frequency. Initial rise in power density is observed due to magnetizing reactance's proportionality with air-gap diameter, but a quick drop in specific power density is again observed for higher pole counts and frequencies.

For permanent magnet synchronous machine, however, the benefit of HFHP topology is shown through finite element analysis. Torque is observed to be reduced by 5% due to reduction in pole pitch with increased pole count, the decrease in weight is observed to outweigh the effect on torque, resulting in a twofold increase in specific power density. By keeping outer diameter as a reference and allowing the air-gap diameter to grow with pole count, a threefold increase in specific power density can be observed.

An example of a high specific power density machine, which is based on the demonstrated benefit of HFHP design on permanent magnet synchronous machine, is presented. The results suggest that secondary effects of HFHP designs, such as increased core loss density and copper losses, can be manageable by adopting additional technologies (Halbach arrays, outer rotor topology, air-gap winding, and Litz wire). Efficiency and specific power density of the motor is shown to be at most 98.3% and 14 kW/kg.

APPENDIX A

INDUCTION MACHINE NO-LOAD TEST AND BLOCKED ROTOR TEST RESULTS

This appendix contains the lab measurements of the no-load test and the blocked rotor test for the baseline, off-the-shelf induction machine for determining the equivalent circuit parameters. Table A.1 shows the no load test measurements and Table A.2 shows the blocked rotor test measurements.

Table A.1: Experimental Results of the No-Load Test

Measurement	Value	Units
Line-to-Line Voltage	205.25	V
Line Current	13.55	A
Total Three Phase Power	240	W
Speed	3596	RPM

Table A.2: Experimental Results of the Blocked Rotor Test

Measurement	Value	Units
Line-to-Line Voltage	46.50	V
Line Current	13.55	A
Total Three Phase Power	461	W
Speed	0	RPM

APPENDIX B

MATLAB CODE FOR SOLVING ELECTRICAL EQUIVALENT INDUCTION MACHINE MODEL

Included in this appendix is the Matlab code written to predict the torque vs. slip curve and the current vs. slip curve.

```
% BASELINE TORQUE = 10.1239 Nm
% BASELINE POWER = 3700 W
% BASELINE SPEED = 3490 RPM
% BASELINE SLIP = 0.03055
% BASELINE RATED CURRENT = 12.3 A

R1_baseline = 0.39;
R2_baseline = 0.35;
X1_baseline = 0.66;
    X_slot = X1_baseline*0.5;
    X_end = X1_baseline*0.3;
    X_ag = X1_baseline*0.2;
X2_baseline = 0.986982;
Rc_baseline = 1e6;
Xm_baseline = 28.41;
srated = 0.03055;
s = 0:0.000001:1;
v1 = 230/sqrt(3);

freq = [60 120 180 240 300 360 420 480 540 600]';
pole = [2 4 6 8 10 12 14 16 18 20]';
R1 = zeros(10,1);
    R1(1,1) = R1_baseline;
X1 = zeros(10,1);
    X1(1,1) = X1_baseline;
R2 = zeros(10,1);
    R2(1,1) = R2_baseline;
X2 = zeros(10,1);
    X2(1,1) = X2_baseline;
```

```
Xm = zeros(10,1);
    Xm(1,1) = Xm_baseline;
Rc = zeros(10,1);
    Rc(1,1) = Rc_baseline;
%Populate the parameters for 10 models
for k = 2:10;
    R1(k,1) = R1_baseline;
    X1(k,1) = (X_slot*(pole(k,1)/2)+...
        X_end*(2/pole(k,1))+X_ag*(2/pole(k,1)));
    R2(k,1) = R2_baseline;
       X2(k,1) = X1(k,1)*X2_baseline/X1_baseline;
    Xm(k,1) = Xm(1,1)/(pole(k,1)/2);
    Rc(k,1) = Rc_baseline;
end

st_s  = zeros(10,1);
shunt  = zeros(10,1);
v_th  = zeros(10,1);
z_th  = zeros(10,1);
Rth  = zeros(10,1);
Xth  = zeros(10,1);

for k = 1:10;
    st_s(k,1) = R1(k,1) + 1i*X1(k,1);
    shunt(k,1) = 1i*Xm(k,1)*Rc(k,1)/...
        (Rc(k,1)+1i*Xm(k,1));
    v_th(k,1) = abs(shunt(k,1)/(shunt(k,1)+...
        st_s(k,1)))*v1;
    z_th(k,1) = shunt(k,1)*st_s(k,1)/...
        (shunt(k,1)+st_s(k,1));
    Rth(k,1) = real(z_th(k,1));
    Xth(k,1) = imag(z_th(k,1));
end

s = 0:0.00001:1;
sz = length(s);
T_2pole = zeros(1,sz);
T_4pole = zeros(1,sz);
T_6pole = zeros(1,sz);
T_8pole = zeros(1,sz);
T_10pole = zeros(1,sz);
T_12pole = zeros(1,sz);
T_14pole = zeros(1,sz);
```

```
T_16pole = zeros(1,sz);
T_18pole = zeros(1,sz);
T_20pole = zeros(1,sz);

for z = 1:sz
T_2pole(1,z) = (3*pole(1,1)/(2*2*pi*freq(1,1)))*...
    (v_th(1,1)^2)*R2(1,1)/s(z)/((Rth(1,1)+R2(1,1)/...
    s(z))^2+(Xth(1,1)+X1(1,1))^2);
T_4pole(1,z) = (3*pole(2,1)/(2*2*pi*freq(2,1)))*...
    (v_th(2,1)^2)*R2(2,1)/s(z)/((Rth(2,1)+R2(2,1)/...
    s(z))^2+(Xth(2,1)+X1(2,1))^2);
T_6pole(1,z) = (3*pole(3,1)/(2*2*pi*freq(3,1)))*...
    (v_th(3,1)^2)*R2(3,1)/s(z)/((Rth(3,1)+R2(3,1)/...
    s(z))^2+(Xth(3,1)+X1(3,1))^2);
T_8pole(1,z) = (3*pole(4,1)/(2*2*pi*freq(4,1)))*...
    (v_th(4,1)^2)*R2(4,1)/s(z)/((Rth(4,1)+R2(4,1)/...
    s(z))^2+(Xth(4,1)+X1(4,1))^2);
T_10pole(1,z) = (3*pole(5,1)/(2*2*pi*freq(5,1)))*...
    (v_th(5,1)^2)*R2(5,1)/s(z)/((Rth(5,1)+R2(5,1)/...
    s(z))^2+(Xth(5,1)+X1(5,1))^2);
T_12pole(1,z) = (3*pole(6,1)/(2*2*pi*freq(6,1)))*...
    (v_th(6,1)^2)*R2(6,1)/s(z)/((Rth(6,1)+R2(6,1)/...
    s(z))^2+(Xth(6,1)+X1(6,1))^2);
T_14pole(1,z) = (3*pole(7,1)/(2*2*pi*freq(7,1)))*...
    (v_th(7,1)^2)*R2(7,1)/s(z)/((Rth(7,1)+R2(7,1)/...
    s(z))^2+(Xth(7,1)+X1(7,1))^2);
T_16pole(1,z) = (3*pole(8,1)/(2*2*pi*freq(8,1)))*...
    (v_th(8,1)^2)*R2(8,1)/s(z)/((Rth(8,1)+R2(8,1)/...
    s(z))^2+(Xth(8,1)+X1(8,1))^2);
T_18pole(1,z) = (3*pole(9,1)/(2*2*pi*freq(9,1)))*...
    (v_th(9,1)^2)*R2(9,1)/s(z)/((Rth(9,1)+R2(9,1)/...
    s(z))^2+(Xth(9,1)+X1(9,1))^2);
T_20pole(1,z) = (3*pole(10,1)/(2*2*pi*freq(10,1)))*...
    (v_th(10,1)^2)*R2(10,1)/s(z)/((Rth(10,1)+R2(10,1)/...
    s(z))^2+(Xth(10,1)+X1(10,1))^2);
end

Zin_2pole = zeros(1,sz);
Zin_4pole = zeros(1,sz);
Zin_6pole = zeros(1,sz);
Zin_8pole = zeros(1,sz);
Zin_10pole = zeros(1,sz);
Zin_12pole = zeros(1,sz);
```

```
Zin_14pole = zeros(1,sz);
Zin_16pole = zeros(1,sz);
Zin_18pole = zeros(1,sz);
Zin_20pole = zeros(1,sz);

I_2pole = zeros(1,sz);
I_4pole = zeros(1,sz);
I_6pole = zeros(1,sz);
I_8pole = zeros(1,sz);
I_10pole = zeros(1,sz);
I_12pole = zeros(1,sz);
I_14pole = zeros(1,sz);
I_16pole = zeros(1,sz);
I_18pole = zeros(1,sz);
I_20pole = zeros(1,sz);

for z = 1:sz
Zin_2pole(1,z) = ((i*X2(1,1)+R2(1,1)/s(z))*...
    (shunt(1,1))/(i*X2(1,1)+R2(1,1)/s(z)+...
    shunt(1,1)))+st_s(1,1);
Zin_4pole(1,z) = ((i*X2(2,1)+R2(2,1)/s(z))*...
    (shunt(2,1))/(i*X2(2,1)+R2(2,1)/s(z)+...
    shunt(2,1)))+st_s(2,1);
Zin_6pole(1,z) = ((i*X2(3,1)+R2(3,1)/s(z))*...
    (shunt(3,1))/(i*X2(3,1)+R2(3,1)/s(z)+...
    shunt(3,1)))+st_s(3,1);
Zin_8pole(1,z) = ((i*X2(4,1)+R2(4,1)/s(z))*...
    (shunt(4,1))/(i*X2(4,1)+R2(4,1)/s(z)+...
    shunt(4,1)))+st_s(4,1);
Zin_10pole(1,z) = ((i*X2(5,1)+R2(5,1)/s(z))*...
    (shunt(5,1))/(i*X2(5,1)+R2(5,1)/s(z)+...
    shunt(5,1)))+st_s(5,1);
Zin_12pole(1,z) = ((i*X2(6,1)+R2(6,1)/s(z))*...
    (shunt(6,1))/(i*X2(6,1)+R2(6,1)/s(z)+...
    shunt(6,1)))+st_s(6,1);
Zin_14pole(1,z) = ((i*X2(7,1)+R2(7,1)/s(z))*...
    (shunt(7,1))/(i*X2(7,1)+R2(7,1)/s(z)+...
    shunt(7,1)))+st_s(7,1);
Zin_16pole(1,z) = ((i*X2(8,1)+R2(8,1)/s(z))*...
    (shunt(8,1))/(i*X2(8,1)+R2(8,1)/s(z)+...
    shunt(8,1)))+st_s(8,1);
Zin_18pole(1,z) = ((i*X2(9,1)+R2(9,1)/s(z))*...
    (shunt(9,1))/(i*X2(9,1)+R2(9,1)/s(z)+...
```

```
    shunt(9,1)))+st_s(9,1);
Zin_20pole(1,z) = ((i*X2(10,1)+R2(10,1)/s(z))*...
    (shunt(10,1))/(i*X2(10,1)+R2(10,1)/s(z)+...
    shunt(10,1)))+st_s(10,1);

I_2pole(1,z) = abs(v1/Zin_2pole(1,z));
I_4pole(1,z) = abs(v1/Zin_4pole(1,z));
I_6pole(1,z) = abs(v1/Zin_6pole(1,z));
I_8pole(1,z) = abs(v1/Zin_8pole(1,z));
I_10pole(1,z) = abs(v1/Zin_10pole(1,z));
I_12pole(1,z) = abs(v1/Zin_12pole(1,z));
I_14pole(1,z) = abs(v1/Zin_14pole(1,z));
I_16pole(1,z) = abs(v1/Zin_16pole(1,z));
I_18pole(1,z) = abs(v1/Zin_18pole(1,z));
I_20pole(1,z) = abs(v1/Zin_20pole(1,z));

k = zeros(10,1);
k(1,1) = find(I_2pole>12.0676,1);
k(2,1) = find(I_4pole>12.0676,1);
k(3,1) = find(I_6pole>12.0676,1);
k(4,1) = find(I_8pole>12.0676,1);
k(5,1) = find(I_10pole>12.0676,1);
k(6,1) = find(I_12pole>12.0676,1);
k(7,1) = find(I_14pole>12.0676,1);
k(8,1) = find(I_16pole>12.0676,1);
k(9,1) = find(I_18pole>12.0676,1);
k(10,1) = find(I_20pole>12.0676,1);

S_rated = zeros(10,1);
S_rated(1,1) = s(1,k(1,1));
S_rated(2,1) = s(1,k(2,1));
S_rated(3,1) = s(1,k(3,1));
S_rated(4,1) = s(1,k(4,1));
S_rated(5,1) = s(1,k(5,1));
S_rated(6,1) = s(1,k(6,1));
S_rated(7,1) = s(1,k(7,1));
S_rated(8,1) = s(1,k(8,1));
S_rated(9,1) = s(1,k(9,1));
S_rated(10,1) = s(1,k(10,1));

T_rated = zeros(10,1);
T_rated(1,1) = T_2pole(1,k(1,1));
T_rated(2,1) = T_4pole(1,k(2,1));
```

```
T_rated(3,1) = T_6pole(1,k(3,1));
T_rated(4,1) = T_8pole(1,k(4,1));
T_rated(5,1) = T_10pole(1,k(5,1));
T_rated(6,1) = T_12pole(1,k(6,1));
T_rated(7,1) = T_14pole(1,k(7,1));
T_rated(8,1) = T_16pole(1,k(8,1));
T_rated(9,1) = T_18pole(1,k(9,1));
T_rated(10,1) = T_20pole(1,k(10,1));
```

APPENDIX C

NUMERICAL RESULTS FOR TORQUE AND CURRENT VS. SLIP

This appendix includes the numerical results obtained from both equivalent circuit method and the finite element analysis.

Table C.1: Analytical Results for the Torque [Nm] vs. Slip

SLIP	2pole	4pole	6pole	8pole	10pole	12pole	14pole	16pole	18pole	20pole
0.001	0.4	0.4	0.3	0.3	0.2	0.2	0.2	0.1	0.1	0.1
0.01	3.7	3.5	3.1	2.7	2.3	1.9	1.6	1.3	1.0	0.8
0.012	4.5	4.2	3.8	3.3	2.8	2.3	1.9	1.5	1.2	1.0
0.014	5.2	4.9	4.4	3.8	3.2	2.6	2.2	1.7	1.4	1.1
0.016	5.9	5.5	5.0	4.3	3.6	3.0	2.4	2.0	1.6	1.3
0.018	6.6	6.2	5.5	4.8	4.0	3.3	2.7	2.2	1.8	1.4
0.02	7.3	6.8	6.1	5.3	4.5	3.7	3.0	2.4	1.9	1.6
0.022	8.0	7.5	6.7	5.8	4.9	4.0	3.3	2.6	2.1	1.7
0.024	8.7	8.1	7.2	6.3	5.3	4.3	3.5	2.8	2.3	1.8
0.026	9.3	8.7	7.8	6.7	5.6	4.6	3.8	3.0	2.4	1.9
0.028	10.0	9.3	8.3	7.2	6.0	4.9	4.0	3.2	2.6	2.0
0.03	10.7	9.9	8.9	7.6	6.4	5.2	4.2	3.4	2.7	2.1
0.032	11.3	10.5	9.4	8.1	6.7	5.5	4.4	3.5	2.8	2.2
0.034	11.9	11.1	9.9	8.5	7.1	5.8	4.6	3.7	2.9	2.3
0.036	12.6	11.7	10.4	8.9	7.4	6.0	4.8	3.8	3.0	2.4
0.038	13.2	12.3	10.9	9.3	7.7	6.3	5.0	4.0	3.1	2.5
0.04	13.8	12.8	11.4	9.7	8.0	6.5	5.2	4.1	3.2	2.5
0.042	14.4	13.4	11.8	10.1	8.3	6.7	5.4	4.2	3.3	2.6
0.044	15.0	13.9	12.3	10.4	8.6	6.9	5.5	4.3	3.4	2.7
0.046	15.6	14.5	12.7	10.8	8.9	7.1	5.7	4.4	3.5	2.7
0.048	16.2	15.0	13.2	11.1	9.1	7.3	5.8	4.5	3.5	2.8
0.05	16.7	15.5	13.6	11.5	9.4	7.5	5.9	4.6	3.6	2.8
0.07	21.9	20.1	17.2	14.2	11.3	8.8	6.7	5.1	3.9	3.0
0.09	26.2	23.7	19.8	15.8	12.2	9.3	7.0	5.2	3.9	2.9
0.12	31.2	27.5	22.1	16.9	12.6	9.2	6.7	4.9	3.6	2.6
0.15	34.6	29.8	23.0	16.9	12.2	8.7	6.2	4.4	3.2	2.3
0.18	36.8	31.0	23.0	16.4	11.5	8.0	5.6	4.0	2.9	2.1
0.2	37.7	31.3	22.8	15.9	10.9	7.6	5.3	3.7	2.7	1.9
0.22	38.3	31.3	22.3	15.3	10.4	7.2	5.0	3.5	2.5	1.8
0.25	38.6	31.0	21.5	14.4	9.7	6.6	4.5	3.2	2.2	1.6
0.3	38.3	29.8	19.9	13.0	8.6	5.8	3.9	2.7	1.9	1.4
0.4	35.8	26.7	16.9	10.7	6.9	4.5	3.1	2.1	1.5	1.1
0.6	29.7	21.0	12.6	7.7	4.8	3.2	2.1	1.4	1.0	0.7
0.8	24.7	17.0	9.9	5.9	3.7	2.4	1.6	1.1	0.8	0.5
1	21.0	14.2	8.1	4.8	3.0	1.9	1.3	0.9	0.6	0.4

Table C.2: Analytical Results for the Current [A] vs. Slip

SLIP	2pole	4pole	6pole	8pole	10pole	12pole	14pole	16pole	18pole	20pole
0.001	4.6	8.8	12.5	15.6	17.9	19.6	20.7	21.3	21.5	21.5
0.01	5.9	9.5	13.0	15.9	18.2	19.8	20.8	21.4	21.6	21.6
0.012	6.4	9.9	13.2	16.1	18.3	19.9	20.9	21.5	21.7	21.6
0.014	6.9	10.2	13.5	16.3	18.5	20.0	21.0	21.6	21.8	21.7
0.016	7.5	10.6	13.8	16.5	18.7	20.2	21.2	21.7	21.9	21.8
0.018	8.1	11.0	14.1	16.8	18.9	20.4	21.3	21.8	22.0	21.9
0.02	8.7	11.5	14.5	17.1	19.1	20.6	21.5	21.9	22.1	21.9
0.022	9.3	12.0	14.8	17.4	19.3	20.8	21.6	22.1	22.2	22.0
0.024	10.0	12.4	15.2	17.7	19.6	21.0	21.8	22.2	22.3	22.1
0.026	10.6	13.0	15.6	18.0	19.9	21.2	22.0	22.4	22.4	22.2
0.028	11.2	13.5	16.1	18.4	20.2	21.4	22.2	22.5	22.5	22.3
0.03	11.9	14.0	16.5	18.7	20.5	21.7	22.4	22.7	22.7	22.4
0.032	12.5	14.6	16.9	19.1	20.8	21.9	22.6	22.8	22.8	22.5
0.034	13.2	15.1	17.4	19.5	21.1	22.2	22.8	23.0	22.9	22.6
0.036	13.8	15.7	17.9	19.8	21.4	22.4	23.0	23.2	23.1	22.7
0.038	14.5	16.3	18.3	20.2	21.7	22.7	23.2	23.3	23.2	22.8
0.04	15.1	16.8	18.8	20.6	22.0	22.9	23.4	23.5	23.3	22.9
0.042	15.8	17.4	19.3	21.0	22.3	23.2	23.6	23.7	23.4	23.0
0.044	16.4	18.0	19.8	21.4	22.7	23.4	23.8	23.8	23.6	23.1
0.046	17.0	18.5	20.3	21.8	23.0	23.7	24.0	24.0	23.7	23.2
0.048	17.7	19.1	20.7	22.2	23.3	23.9	24.2	24.1	23.8	23.3
0.05	18.3	19.6	21.2	22.6	23.6	24.2	24.4	24.3	23.9	23.4
0.07	24.3	25.1	25.8	26.3	26.5	26.4	26.1	25.5	24.9	24.1
0.09	29.7	30.0	29.8	29.4	28.8	28.1	27.3	26.4	25.5	24.6
0.12	36.7	36.1	34.6	32.9	31.3	29.8	28.5	27.2	26.1	25.0
0.15	42.6	41.1	38.1	35.3	32.9	30.9	29.2	27.7	26.4	25.2
0.18	47.4	45.0	40.8	37.0	34.0	31.7	29.7	28.0	26.6	25.3
0.2	50.2	47.1	42.1	37.9	34.6	32.0	29.9	28.2	26.7	25.4
0.22	52.6	48.9	43.3	38.6	35.0	32.3	30.1	28.3	26.8	25.5
0.25	55.7	51.2	44.7	39.4	35.5	32.6	30.3	28.4	26.9	25.5
0.3	59.8	54.1	46.3	40.4	36.1	32.9	30.5	28.6	27.0	25.6
0.4	65.3	57.8	48.3	41.5	36.7	33.3	30.7	28.7	27.1	25.6
0.6	70.8	61.3	50.1	42.4	37.2	33.6	30.9	28.8	27.1	25.7
0.8	73.5	62.9	50.8	42.8	37.5	33.7	31.0	28.9	27.2	25.7
1	75.0	63.7	51.3	43.0	37.6	33.8	31.1	28.9	27.2	25.7

Table C.3: FEA Results for the Torque [Nm] vs. Slip

Slip	2pole	4pole	6pole	8pole	10pole	12pole	14pole	16pole	18pole	20pole
0.001	0.4	0.4	0.3	0.3	0.3	0.3	0.3	0.2	0.2	0.2
0.01	3.5	3.5	3.3	3.2	3.0	2.8	2.5	2.3	2.1	1.9
0.012	4.2	4.1	4.0	3.8	3.5	3.3	3.0	2.7	2.5	2.2
0.014	4.9	4.8	4.6	4.4	4.1	3.8	3.5	3.2	2.9	2.6
0.016	5.6	5.4	5.2	5.0	4.6	4.3	3.9	3.6	3.2	2.9
0.018	6.2	6.1	5.8	5.5	5.2	4.8	4.4	4.0	3.6	3.2
0.02	6.9	6.7	6.5	6.1	5.7	5.3	4.8	4.4	3.9	3.5
0.022	7.5	7.4	7.1	6.7	6.2	5.7	5.3	4.8	4.3	3.8
0.024	8.2	8.0	7.6	7.2	6.7	6.2	5.7	5.1	4.6	4.1
0.026	8.8	8.6	8.2	7.7	7.2	6.6	6.1	5.5	4.9	4.4
0.028	9.4	9.2	8.8	8.3	7.7	7.1	6.4	5.8	5.2	4.6
0.03	10.0	9.8	9.3	8.8	8.2	7.5	6.8	6.1	5.5	4.8
0.032	10.6	10.3	9.9	9.3	8.6	7.9	7.1	6.4	5.7	5.1
0.034	11.2	10.9	10.4	9.8	9.0	8.3	7.5	6.7	6.0	5.3
0.036	11.8	11.5	10.9	10.2	9.5	8.6	7.8	7.0	6.2	5.4
0.038	12.3	12.0	11.4	10.7	9.9	9.0	8.1	7.2	6.4	5.6
0.04	12.9	12.6	11.9	11.1	10.3	9.3	8.4	7.5	6.6	5.8
0.042	13.4	13.1	12.4	11.6	10.6	9.6	8.7	7.7	6.8	5.9
0.044	14.0	13.6	12.9	12.0	11.0	10.0	8.9	7.9	6.9	6.1
0.046	14.5	14.1	13.3	12.4	11.3	10.2	9.2	8.1	7.1	6.2
0.048	15.0	14.6	13.8	12.8	11.7	10.5	9.4	8.3	7.2	6.3
0.05	15.5	15.1	14.2	13.2	12.0	10.8	9.6	8.5	7.4	6.4
0.07	20.1	19.3	17.9	16.3	14.5	12.7	11.1	9.5	8.2	6.9
0.09	23.7	22.6	20.6	18.2	15.9	13.7	11.6	9.9	8.3	6.9
0.12	27.5	25.8	22.8	19.7	16.6	13.9	11.6	9.6	7.9	6.6
0.15	29.9	27.5	23.8	19.9	16.4	13.5	11.1	9.1	7.4	6.1
0.18	31.1	28.2	23.8	19.5	15.8	12.8	10.4	8.5	7.0	5.7
0.2	31.5	28.3	23.6	19.1	15.4	12.4	10.0	8.2	6.7	5.5
0.22	31.7	28.2	23.2	18.6	14.9	11.9	9.6	7.9	6.4	5.3
0.25	31.5	27.7	22.4	17.8	14.2	11.3	9.2	7.5	6.1	5.1
0.3	30.7	26.4	21.1	16.6	13.1	10.5	8.5	7.0	5.8	4.9
0.4	28.0	23.6	18.5	14.5	11.5	9.4	7.7	6.5	5.5	4.7
0.6	22.7	19.0	15.1	12.1	10.0	8.4	7.2	6.3	5.5	4.8
0.8	18.8	16.1	13.2	11.1	9.5	8.3	7.3	6.4	5.7	5.0
1	16.1	14.3	12.3	10.7	9.4	8.4	7.5	6.7	5.9	5.3

Table C.4: FEA Results for the Current [A] vs. Slip

Slip	2pole	4pole	6pole	8pole	10pole	12pole	14pole	16pole	18pole	20pole
0.001	4.8	7.8	10.8	13.7	16.3	18.7	20.9	22.8	24.4	25.8
0.01	5.9	8.6	11.4	14.1	16.6	19.0	21.1	23.0	24.6	26.0
0.012	6.3	8.9	11.6	14.3	16.8	19.2	21.2	23.1	24.7	26.1
0.014	6.8	9.3	11.9	14.5	17.0	19.3	21.4	23.2	24.8	26.2
0.016	7.3	9.7	12.2	14.8	17.3	19.6	21.6	23.4	25.0	26.3
0.018	7.9	10.1	12.6	15.1	17.5	19.8	21.8	23.6	25.2	26.5
0.02	8.4	10.6	13.0	15.5	17.8	20.1	22.1	23.8	25.4	26.7
0.022	9.0	11.1	13.4	15.8	18.2	20.3	22.3	24.1	25.6	26.9
0.024	9.6	11.6	13.8	16.2	18.5	20.6	22.6	24.3	25.8	27.1
0.026	10.2	12.1	14.3	16.6	18.8	21.0	22.9	24.6	26.0	27.3
0.028	10.8	12.6	14.8	17.0	19.2	21.3	23.2	24.8	26.3	27.5
0.03	11.4	13.2	15.2	17.4	19.6	21.6	23.5	25.1	26.5	27.7
0.032	12.0	13.7	15.7	17.9	20.0	22.0	23.8	25.4	26.8	28.0
0.034	12.6	14.3	16.2	18.3	20.4	22.4	24.1	25.7	27.1	28.2
0.036	13.2	14.8	16.8	18.8	20.8	22.7	24.5	26.0	27.3	28.5
0.038	13.8	15.4	17.3	19.3	21.2	23.1	24.8	26.3	27.6	28.7
0.04	14.4	16.0	17.8	19.7	21.7	23.5	25.2	26.6	27.9	28.9
0.042	15.0	16.5	18.3	20.2	22.1	23.9	25.5	26.9	28.2	29.2
0.044	15.6	17.1	18.8	20.7	22.5	24.3	25.9	27.2	28.4	29.4
0.046	16.2	17.7	19.4	21.2	23.0	24.7	26.2	27.6	28.7	29.7
0.048	16.8	18.2	19.9	21.6	23.4	25.0	26.5	27.9	29.0	29.9
0.05	17.4	18.8	20.4	22.1	23.8	25.4	26.9	28.2	29.3	30.1
0.07	23.2	24.3	25.5	26.8	28.0	29.1	30.1	31.0	31.7	32.2
0.09	28.4	29.3	30.1	30.9	31.6	32.3	32.8	33.3	33.6	33.8
0.12	35.3	35.8	35.9	35.9	35.9	35.9	35.8	35.7	35.6	35.5
0.15	41.2	41.2	40.5	39.8	39.0	38.4	37.8	37.4	36.9	36.5
0.18	46.2	45.6	44.2	42.7	41.3	40.2	39.3	38.5	37.8	37.2
0.2	49.0	48.1	46.2	44.2	42.5	41.1	40.0	39.0	38.2	37.5
0.22	51.6	50.3	47.9	45.5	43.5	41.9	40.6	39.5	38.6	37.8
0.25	54.9	53.0	50.0	47.1	44.7	42.8	41.2	40.0	39.0	38.2
0.3	59.4	56.7	52.7	49.1	46.2	43.9	42.1	40.7	39.5	38.6
0.4	65.6	61.4	56.1	51.5	47.9	45.2	43.1	41.5	40.2	39.2
0.6	72.2	66.3	59.4	53.9	49.7	46.7	44.4	42.6	41.2	40.1
0.8	75.6	68.6	61.1	55.2	50.9	47.7	45.3	43.5	42.1	40.9
1	77.5	70.0	62.1	56.1	51.8	48.6	46.2	44.4	42.9	41.6

REFERENCES

[1] J. C. Michalowicz, "Origin of the electric motor," *American Institute of Electrical Engineers, Transactions of the*, vol. 67, no. 2, pp. 1288–1292, January 1948.

[2] M. D. Hathaway, R. D. Rosario, and N. K. Madavan, "NASA fixed wing project propulsion research and technology development activities to reduce thrust specific energy consumption," National Aeronautics and Space Administration, Tech. Rep., 2013.

[3] B. Sarlioglu and C. Morris, "More electric aircraft-review, challenges and opportunities for commercial transport aircraft," *IEEE Transactions on Transportation Electrification*, vol. 1, no. 1, pp. 54–64, 2015.

[4] International Air Transport Association, "Vision 2050," 2011. [Online]. Available: https://www.iata.org/pressroom/facts_figures/Documents/vision-2050.pdf

[5] European-Commission, "Reducing emissions from aviation." [Online]. Available: http://ec.europa.eu/clima/policies/transport/aviation/index_en.htm

[6] C. Thompson, "Elon musk says Tesla will dramatically increase the range of its cars by 2020." [Online]. Available: http://www.techinsider.io/elon-musk-says-tesla-car-range-will-increase-2015-9

[7] National Aeronautics and Space Administration, "Advanced air vehicles program, advanced air transport technology project," September 2014, fixed wing/advanced air transport Technology project overview, NRA Kick-off meeting, Cleveland, OH.

[8] J. Felder, H. Kim, and G. Brown, *Turboelectric Distributed Propulsion Engine Cycle Analysis for Hybrid-Wing-Body Aircraft.* American Institute of Aeronautics and Astronautics, 2016/02/08 2009. [Online]. Available: http://dx.doi.org/10.2514/6.2009-1132

[9] R. Bates, C. Cosad, L. Fielder, A. Kosmala, S. Hudson, G. Romero, and V. Shanmugam, "Taking the pulse of producing wells - ESP surveillance," *Oilfield Review*, vol. 16, 2004.

[10] X. Liang and E. Fleming, "Electrical submersible pump systems: Evaluating their power consumption," *Industry Applications Magazine, IEEE*, vol. 19, no. 6, pp. 46–55, 2013.

[11] T. J. Miller, *SPEED's Electric Motors: An Outline of Some of the Theory in the SPEED Software for Electric Machine Design: with Problems and Solutions*. Magna Physics, 2004.

[12] P. L. Alger, *Induction Machines: Their Behavior and Uses*. Gordon and Breach Science Publishers, 1970.

[13] Y. Chen and P. Pillay, "An improved formula for lamination core loss calculations in machines operating with high frequency and high flux density excitation," in *Industry Applications Conference, 2002. 37th IAS Annual Meeting. Conference Record of the*, 2002.

[14] Z. Q. Zhu and D. Howe, "Halbach permanent magnet machines and applications: A review," *IEE Proceedings = Electric Power Appliocations*, vol. 148, no. 4, pp. 299–308, 2001.

[15] Y. Hu, T. Wu, L. Chow, Y. Bai, and W. Wu, "Design of a 3kw 150k rpm super high-speed permanent magnet synchronous motor," in *Electrical Machines (ICEM), 2014 International Conference on*, 2014, pp. 2543–2548.

[16] "IEEE standard test procedure for polyphase induction motors and generators," *IEEE Std 112-2004 (Revision of IEEE Std 112-1996)*, 2004.

[17] A. Yoon, X. Yi, J. Martin, Y. Chen, and K. Haran, "A high-speed, high-frequency, air-core pm machine for aircraft application," in *Power and Energy Conference at Illinois (PECI), 2016 IEEE*, 2016.